








TECH BRIEFS

NATIONAL AERONAUTICS AND SPACE ADMINISTRATION

-  **Technology Focus**
-  **Computers/Electronics**
-  **Software**
-  **Materials**
-  **Mechanics**
-  **Machinery/Automation**
-  **Manufacturing**
-  **Bio-Medical**
-  **Physical Sciences**
-  **Information Sciences**
-  **Books and Reports**

INTRODUCTION

Tech Briefs are short announcements of innovations originating from research and development activities of the National Aeronautics and Space Administration. They emphasize information considered likely to be transferable across industrial, regional, or disciplinary lines and are issued to encourage commercial application.

Availability of NASA Tech Briefs and TSPs

Requests for individual Tech Briefs or for Technical Support Packages (TSPs) announced herein should be addressed to

National Technology Transfer Center

Telephone No. (800) 678-6882 or via World Wide Web at www2.nttc.edu/leads/

Please reference the control numbers appearing at the end of each Tech Brief. Information on NASA's Commercial Technology Team, its documents, and services is also available at the same facility or on the World Wide Web at www.nctn.hq.nasa.gov.

Commercial Technology Offices and Patent Counsels are located at NASA field centers to provide technology-transfer access to industrial users. Inquiries can be made by contacting NASA field centers and program offices listed below.

NASA Field Centers and Program Offices

Ames Research Center

Lisa L. Lockyer
(650) 604-3009
lisa.l.lockyer@nasa.gov

Dryden Flight Research Center

Gregory Poteat
(661) 276-3872
greg.poteat@dfrc.nasa.gov

Goddard Space Flight Center

Nona Cheeks
(301) 286-5810
Nona.K.Cheeks.1@gsfc.nasa.gov

Jet Propulsion Laboratory

Ken Wolfenbarger
(818) 354-3821
james.k.wolfenbarger@jpl.nasa.gov

Johnson Space Center

Charlene E. Gilbert
(281) 483-3809
commercialization@jsc.nasa.gov

Kennedy Space Center

Jim Aliberti
(321) 867-6224
Jim.Aliberti-1@ksc.nasa.gov

Langley Research Center

Jesse Midgett
(757) 864-3936
jesse.c.midgett@nasa.gov

John H. Glenn Research Center at Lewis Field

Larry Viterna
(216) 433-3484
cto@grc.nasa.gov

Marshall Space Flight Center

Vernotto McMillan
(256) 544-2615
vernotto.mcmillan@msfc.nasa.gov

Stennis Space Center

Robert Bruce
(228) 688-1929
robert.c.bruce@nasa.gov

NASA Program Offices

At NASA Headquarters there are seven major program offices that develop and oversee technology projects of potential interest to industry:

Carl Ray

Small Business Innovation Research Program (SBIR) & Small Business Technology Transfer Program (STTR)
(202) 358-4652 or
cray@nasa.gov

Benjamin Neumann

Innovative Technology Transfer Partnerships (Code TD)
(202) 358-2320
benjamin.j.neumann@nasa.gov

John Mankins

Office of Space Flight (Code TD)
(202) 358-4659 or
john.c.mankins@nasa.gov

Terry Hertz

Office of Aero-Space Technology (Code RS)
(202) 358-4636 or
thertz@nasa.gov

Glen Mucklow

Office of Space Sciences (Code SM)
(202) 358-2235 or
gmucklow@nasa.gov

Roger Crouch

Office of Microgravity Science Applications (Code U)
(202) 358-0689 or
rcrouch@nasa.gov

Granville Paules

Office of Mission to Planet Earth (Code Y)
(202) 358-0706 or
gpaules@mtpe.hq.nasa.gov



TECH BRIEFS

NATIONAL AERONAUTICS AND SPACE ADMINISTRATION



5 Technology Focus: Test & Measurement

- 5 Multifunction Imaging and Spectroscopic Instrument
- 6 Position-Finding Instrument Built Around a Magnetometer
- 6 Improved Measurement of Dispersion in an Optical Fiber
- 7 Probe for Sampling of Interstitial Fluid From Bone
- 8 Neuropsychological Testing of Astronauts
- 8 Method of Calibration for a Large Cathetometer System



9 Electronics/Computers

- 9 Four-Channel PC/104 MIL-STD-1553 Circuit Board
- 9 Improved Method of Locating Defects in Wiring Insulation
- 10 Strobe Traffic Lights Warn of Approaching Emergency Vehicles
- 11 Improved Timing Scheme for Spaceborne Precipitation Radar
- 12 Concept for Multiple-Access Free-Space Laser Communications
- 13 Variable Shadow Screens for Imaging Optical Devices



15 Software

- 15 Verifying Diagnostic Software
- 15 Initial Processing of Infrared Spectral Data
- 15 Activity-Centric Approach to Distributed Programming
- 15 Controlling Distributed Planning



17 Materials

- 17 New Material for Surface-Enhanced Raman Spectroscopy
- 17 Treated Carbon Nanofibers for Storing Energy in Aqueous KOH



19 Mechanics

- 19 Advanced Infant Car Seat Would Increase Highway Safety



21 Machinery/Automation

- 21 Development of Biomimetic Flyers
- 21 Second-Generation Six-Limbed Experimental Robot
- 22 Miniature Linear Actuator for Small Spacecraft



23 Manufacturing

- 23 Process for Making Single-Domain Magnetite Crystals
- 24 A New Process for Fabricating Random Silicon Nanotips
- 25 Resin-Transfer-Molding of a Tool Face
- 25 Improved Phase-Mask Fabrication of Fiber Bragg Gratings
- 26 Tool for Insertion of a Fiber-Optic Terminus in a Connector



27 Physical Sciences

- 27 Nanofluidic Size-Exclusion Chromatograph
- 28 Lightweight, Low-CTE Tubes Made From Biaxially Oriented LCPs
- 28 Using Redundancy To Reduce Errors in Magnetometer Readings
- 29 Compact Instrument for Measuring Profile of a Light Beam
- 30 Multilayer Dielectric Transmissive Optical Phase Modulator
- 31 Second-Generation Multi-Angle Imaging Spectroradiometer



33 Information Sciences

- 33 Real-Time Adaptive Color Segmentation by Neural Networks



35 Books & Reports

- 35 Research and Development in Optical Communications
- 35 Tests of Multibeam Scintillation Mitigation on Laser Uplinks
- 35 Spaceborne Infrared Atmospheric Sounder

This document was prepared under the sponsorship of the National Aeronautics and Space Administration. Neither the United States Government nor any person acting on behalf of the United States Government assumes any liability resulting from the use of the information contained in this document, or warrants that such use will be free from privately owned rights.



Multifunction Imaging and Spectroscopic Instrument

There would be no repositioning for different observations of the same specimen.

NASA's Jet Propulsion Laboratory, Pasadena, California

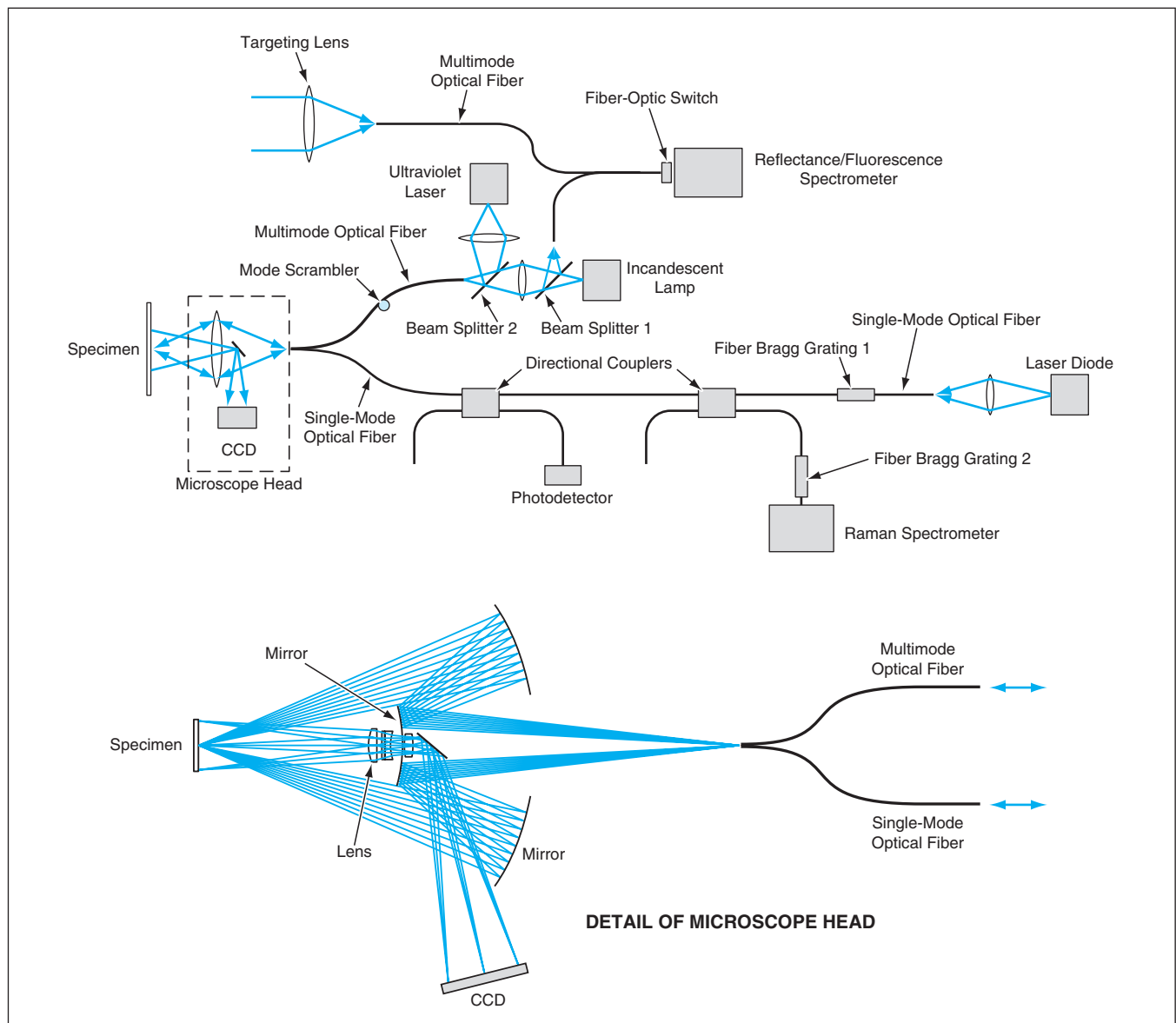
A proposed optoelectronic instrument would perform several different spectroscopic and imaging functions that, heretofore, have been performed by separate instruments. The functions would be reflectance, fluorescence, and Raman spectroscopies; variable-color confocal imaging at two different resolutions; and wide-field color imaging.

The instrument was conceived for use in examination of minerals on remote

planets. It could also be used on Earth to characterize material specimens. The conceptual design of the instrument emphasizes compactness and economy, to be achieved largely through sharing of components among subsystems that perform different imaging and spectrometric functions. The input optics for the various functions would be mounted in a single optical head. With the exception of a targeting lens, the input optics

would all be aimed at the same spot on a specimen, thereby both (1) eliminating the need to reposition the specimen to perform different imaging and/or spectroscopic observations and (2) ensuring that data from such observations can be correlated with respect to known positions on the specimen.

The figure schematically depicts the principal components and subsystems of the instrument. The targeting lens



A **Single Instrument** would incorporate multiple subsystems that would share optical components.

would collect light into a multimode optical fiber, which would guide the light through a fiber-selection switch to a reflection/fluorescence spectrometer. The switch would have four positions, enabling selection of spectrometer input from the targeting lens, from either of one or two multimode optical fibers coming from a reflectance/fluorescence-microspectrometer optical head, or from a dark calibration position (no fiber). The switch would be the only moving part within the instrument.

For reflection spectroscopy, light from an incandescent lamp would be focused onto another multimode optical fiber, would pass through a mode scrambler, and would illuminate the specimen through a microscope head. Light reflected from the specimen would be collected through the same optical fiber and would be directed into the reflection/fluorescence spectrometer via beam splitter 1. To illuminate the specimen for fluorescence spectroscopy, light from an ultravi-

olet laser would be directed, via beam splitter 2, into the same optical fiber used to illuminate the specimen for reflectance spectroscopy. The fluorescent light from the specimen would be collected and sent to the reflection/fluorescence spectrometer in the same manner as that of the reflected light.

For Raman spectroscopy, light from a laser diode would be focused onto a single-mode optical fiber and would pass through fiber Bragg grating 1, which would lock the wavelength. This light would be guided through two directional couplers to the microscope head. Raman-shifted light captured by the lens would be collected through the same single-mode optical fiber, and would be guided to the Raman spectrometer through one of the directional couplers and fiber Bragg grating 2, which would reject the reflected (unshifted) light. The Raman spectrometer and its associated optical components were described in "Confocal Single-Mode-Fiber-Optic

Raman Microspectrometer" (NPO-20932), *NASA Tech Briefs*, Vol. 25, No. 4 (April 2001), page 10a.

The imaging portion of the instrument would include a charge-coupled-device (CCD) color camera, which would be used to provide contextual information for the point-imaging (confocal) subsystems. The lens for this camera and the lens for confocal imaging would be different but integrated into a single unit in the microscope head, as depicted in the detail at the bottom of the figure. The aforementioned multimode optical fiber used for reflection and fluorescence spectroscopy and the aforementioned single-mode optical fiber used for Raman spectroscopy would also be used for confocal imaging at a lower and a higher resolution, respectively.

This work was done by Pantazis Mouroulis of Caltech for NASA's Jet Propulsion Laboratory. Further information is contained in a TSP (see page 1). NPO-30650

Position-Finding Instrument Built Around a Magnetometer

A coarse indication of position is derived from a relatively inexpensive instrument.

Goddard Space Flight Center, Greenbelt, Maryland

A coarse-positioning instrument is built around a three-axis magnetometer. The magnetometer is of a type that is made of inexpensive hardware and is suitable for use aboard spacecraft orbiting no more than 1,000 km above the surface of the Earth. A data processor programmed with suitable software and equipped with a central processing unit, random-access memory, programmable read-only memory, and interface circuitry for communication with external equipment are added to the basic magnetometer to convert it into a coarse-positioning instrument. Although the instrument was conceived for use aboard spacecraft, it could

be useful for navigation on Earth under some circumstances.

A major feature of the proposed instrument is an ability to generate a coarse estimate of its position in real time (that is, without start-up delay). Algorithms needed to solve the position equations have been developed. These include algorithms to work around gaps in measurement data that arise from a singularity near the minimum in the magnetic field of the Earth.

Some work has been done to develop a prototype of this instrument incorporating a standard three-axis flux-gate magnetometer and a Pentium P-5 (or equiva-

lent) processor with a clock frequency of 120 MHz. Alternatively, the processor could be of the '486 class. A computer model of the instrument has been completed and tested.

This work was done by Eleanor Ketchum of Goddard Space Flight Center. Further information is contained in a TSP (see page 1).

This invention has been patented by NASA (U.S. Patent No. 6,114,995). Inquiries concerning nonexclusive or exclusive license for its commercial development should be addressed to the Patent Counsel, Goddard Space Flight Center; (301) 286-7351. Refer to GSC-13880.

Improved Measurement of Dispersion in an Optical Fiber

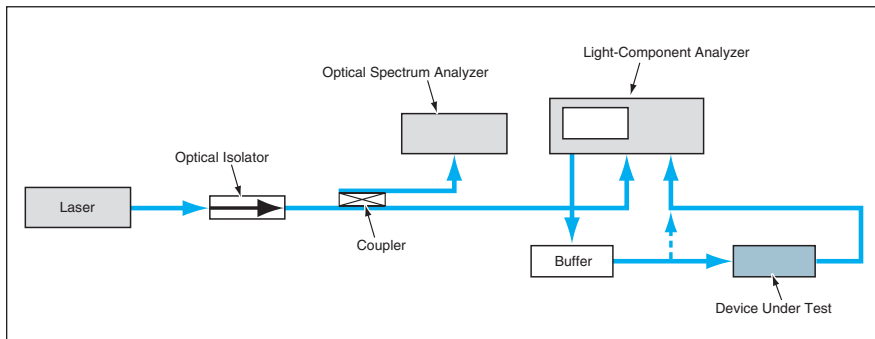
The lower limit of measurability is extended.

NASA's Jet Propulsion Laboratory, Pasadena, California

An improved method of measuring chromatic dispersion in an optical fiber or other device affords a lower (relative to prior such methods) limit of measurable dispersion. This method is a modified ver-

sion of the amplitude-modulation (AM) method, which is one of the prior methods. In comparison with the other prior methods, the AM method is less complex. However, the AM method is limited to dis-

persion levels ≥ 160 ps/nm and cannot be used to measure the symbol of the dispersion. In contrast, the present modified version of the AM method can be used to measure the symbol of the symbol of the



This Apparatus for Measuring Dispersion in the device under test is the same as that used in the unmodified AM method, except for the inclusion of the buffer.

dispersion and affords a measurement range from about 2 ps/nm to several thousand ps/nm with a resolution of 0.27 ps/nm or finer.

The figure schematically depicts the measurement apparatus. The source of light for the measurement is a laser, the wavelength of which is monitored by an optical spectrum analyzer. A light-component analyzer amplitude-modulates the light with a scanning radio-frequency signal. The modulated light is passed through a buffer (described below) and through the device under test (e.g., an optical fiber, the dispersion of which one seeks to measure), then back to the light-component analyzer for spectrum analysis.

Dispersion in the device under test gives rise to phase shifts among the carrier and the upper and lower sideband components of the modulated signal. These phase shifts affect the modulation-frequency component of the output of a photodetector exposed to the signal that emerges from the device under test. One of the effects is that this component goes to zero periodically as the modulation frequency is varied. From the basic equations

for dispersion of the modulated signal and the amplitude of the modulation-frequency output of the photodetector, the following equation has been derived:

$$D_T = \frac{(2n-1)c}{2\lambda^2 f_n^2},$$

where D_T is the total dispersion, n is an integer, c is the speed of light, λ is the laser wavelength, and f_n is the n th modulation frequency for which the photodetector output vanishes.

One of the conclusions that one can draw from the foregoing equation is that the lower limit of measurability in the AM method is set by the highest modulation frequency. For example, in the case of an apparatus that lacks a buffer but is otherwise identical to that shown in the figure and that has a maximum modulation frequency of 20 GHz and a laser wavelength of 1,550 nm, the minimum measurable dispersion is about 160 ps/nm.

What distinguishes the present method is the inclusion of the buffer, which can be an optical fiber, a fiber-optic grating or a combination of the two. The buffer must have a known dis-

persion, D_B , approximately equal to or larger than the minimum measurable dispersion. One can determine D_B from a measurement performed without the device under test (that is, the buffer only) in the optical train. When both the buffer and the device under test are present, the total dispersion is given by

$$D_T = D_B + D_{DUT} = \frac{(2n-1)c}{2\lambda^2 f_n^2},$$

where D_{DUT} is the dispersion of the device under test. Then

$$D_{DUT} = D_T - D_B = \frac{(2n-1)c}{2\lambda^2 f_n^2} - D_B.$$

By virtue of the subtraction of D_B , the lower limit of measurability of D_{DUT} is lower than that of D_T . If the symbol of the dispersion is small, one can obtain it by measuring the change in f_n (df_n) and then calculating it approximately as the differential of the immediately preceding equation:

$$dD_T = -2D_T df_n / f_n.$$

This work was done by Shouhua Huang, Thanh Le, and Lute Maleki of Caltech for NASA's Jet Propulsion Laboratory. Further information is contained in a TSP (see page 1).

In accordance with Public Law 96-517, the contractor has elected to retain title to this invention. Inquiries concerning rights for its commercial use should be addressed to:

*Innovative Technology Assets Management
JPL*

*Mail Stop 202-233
4800 Oak Grove Drive
Pasadena, CA 91109-8099
(818) 354-2240*

E-mail: iaoffice@jpl.nasa.gov

Refer to NPO-30406, volume and number of this NASA Tech Briefs issue, and the page number.

Probe for Sampling of Interstitial Fluid From Bone

Lyndon B. Johnson Space Center, Houston, Texas

An apparatus characterized as both a membrane probe and a bone ultrafiltration probe has been developed to enable *in vivo* sampling of interstitial fluid in bone. The probe makes it possible to measure the concentration of calcium and other constituents of the fluid that may be relevant to bone physiology. The probe could be especially helpful in experimental studies of microgravitational bone loss and of terrestrial bone-loss disease states, including osteoporosis.

The probe can be implanted in the bone tissue of a living animal and can be used to extract samples of the interstitial bone fluid from time to time during a long-term study. The probe includes three 12-cm-long polyacrylonitrile fibers configured in a loop form and attached to polyurethane tubing [inside diameter 0.025 in. (0.64 mm), outside diameter 0.040 in. (1 mm)]; the attachment is made by use of a 1-cm-long connecting piece of polyurethane tubing [inside diameter 0.035±0.003 in. (0.89±0.08 mm), outside diameter 0.060±0.003 in.

(1.52±0.08 mm)]. At the distal end, a 2-cm-long piece of polyurethane tubing of the same inner and outer diameters serves as a connector to a hub. A 1-cm-long piece of expanded poly (tetrafluoroethylene) tubing over the joint between the fibers and the connecting tubing serves as a tissue-ingrowth site.

This work was done by Elsa M. Janle of Bioanalytical Systems, Inc., for Johnson Space Center. For further information, contact the Johnson Commercial Technology Office at (281) 483-3809. MSC-23044

Neuropsychological Testing of Astronauts

Lyndon B. Johnson Space Center, Houston, Texas

The Spaceflight Cognitive Assessment Tool for Windows (WinSCAT) is a computer program that administers a battery of five timed neuro-cognitive tests. WinSCAT was developed to give astronauts an objective and automated means of assessing their cognitive functioning during space flight, as compared with their own baseline performances measured during similar prior testing on the ground. WinSCAT is also intended for use by flight surgeons to assess cognitive impairment after exposure of astronauts to such cognitive assaults as head trauma, decompression sickness, and exposure to toxic gas. The

tests were selected from among a group of tests, denoted the Automated Neuropsychological Assessment Metrics, that were created by the United States Navy and Army for use in evaluating the cognitive impairment of military personnel who have been subjected to medication or are suspected to have sustained brain injuries. These tests have been validated in a variety of clinical settings and are now in the public domain. The tests are presented in a Microsoft Windows shell that facilitates administration and enables immediate reporting of test scores in numerical and graphical forms.

This program was written by Christopher Flynn of Johnson Space Center and Steve Vander Ark, Daniel Eksuzian, Walter Sipes, Robert Kane, Rodney Vanderploeg, Paul Retzlaff, Tim Elsmore, and Jeffrey Moore of Wyle Laboratories. For further information, contact:

Wyle Laboratories
Life Sciences Division
1290 Hercules Dr. Suite 120
Houston, TX 77058
Telephone No. (281) 212-1200
www.wyllabs.com
Refer to MSC-23332.

Method of Calibration for a Large Cathetometer System

This method costs considerably less than does a prior method

Goddard Space Flight Center, Greenbelt, Maryland

A method of calibration has been devised for a pair of mutually orthogonal two-axis cathetometers that, when used together, yield measurements of three-dimensional positions of objects mounted on an optical bench. Each cathetometer has a horizontal travel of 1.8 m and a vertical travel of 1.2 m. The cathetometers are required to measure X, Y, and Z coordinates (see figure) to within ± 0.005 in. (± 0.127 mm).

Each cathetometer consists of an alignment telescope on a platform mounted on a two-dimensional translation stage. The knowledge required for calibration of each cathetometer is (1) the two-dimensional position of the cathetometer platform as a function of the electronic readouts of position encoders on the

translation stage and (2) the amount of any angular misalignment (roll, pitch, and/or yaw) of the cathetometer platform as a function of the two-dimensional coordinates or the position-encoder readouts. By use of three equations derived from the applicable trigonometric relationships, the calibrated X, Y, and Z coordinates can be computed from the raw encoder readouts.

The calibration measurements are performed by use of two main tools: a laser ranging interferometer and an electronic level that provides a gravity reference. The laser ranging interferometer is used to measure the yaw and roll of the X-Z cathetometer and the yaw and pitch of the Y-Z cathetometer. The laser ranging interferometer is also used to calibrate the position encoders. The electronic level gives a gravity reference for the interferometer measurements and for aligning the Z axis as close as possible to vertical. The interferometer is precise to within 0.01 arc seconds, and the level is precise to within 0.2 arc seconds. Once the calibration measurements have been completed and until a recalibration is required, it is not necessary to use the interferometer and level to monitor the cathetometers during operation.

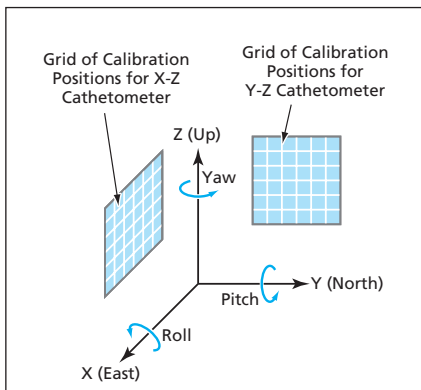
The calibration measurements for each cathetometer are performed on a two-dimensional grid of positions at increments

of 20 mm. For intermediate positions, angular-misalignment data and the uncertainties in those data are obtained by use of a bilinear interpolation scheme that is amenable to rapid calculation. The raw calibration measurement data are stored in text files in a computer. Software written specifically for the purpose performs the interpolation and the conversion of raw encoder outputs to calibrated X, Y, and Z coordinates in real time.

Tests have shown that the uncertainty in the calibration satisfies the ± 0.005 -in. (± 0.127 -mm) requirement. This is comparable to the uncertainties of laser trackers and theodolites.

A prior calibration method that affords the requisite accuracy is time-consuming, requires at least two technicians, and involves the use of custom-made scales and tooling bars in conjunction with constant monitoring of the cathetometers during operation by use of a displacement-measuring interferometer. In contrast, the present method can be implemented by a single technician, takes less time, and does not require constant use of an interferometer. The net result is that the present method costs several hundred thousand dollars less.

This work was done by Ronald Toland of Goddard Space Flight Center. Further information is contained in a TSP (see page 1). GSC-14741-1



X, Y, and Z Coordinates are measured by combined use of an X-Z and Y-Z cathetometer.



Four-Channel PC/104 MIL-STD-1553 Circuit Board

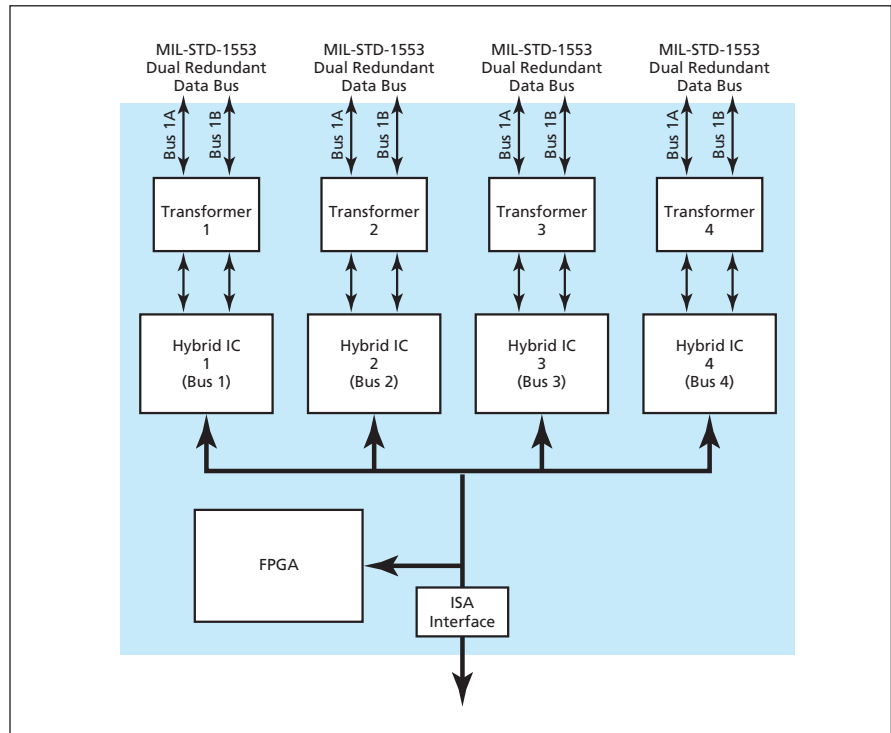
For a given size, weight, and power consumption, greater functionality is obtained.

Lyndon B. Johnson Space Center, Houston, Texas

The mini bus interface card (miniBIC) is the first four-channel electronic circuit board that conforms to MIL-STD-1553 and to the electrical-footprint portion of PC/104. [MIL-STD-1553 is a military standard that encompasses a method of communication and electrical-interface requirements for digital electronic subsystems connected to a data bus. PC/104 is an industry standard for compact, stackable modules that are fully compatible (in architecture, hardware, and software) with personal-computer data- and power-bus circuitry.]

Prior to the development of the miniBIC, only one- and two-channel PC/104 MIL-STD-1553 boards were available. To obtain four channels, it was necessary to include at least two boards in a PC/104 stack. In comparison with such a two-board stack, the miniBIC takes up less space, consumes less power, and is more reliable. In addition, the miniBIC includes 32 digital input/output channels.

The miniBIC (see figure) contains four MIL-STD-1553B hybrid integrated circuits (ICs), four transformers, a field-programmable gate array (FPGA), and an Industry Standard Architecture (ISA) interface. Each hybrid IC includes a MIL-STD-1553 dual transceiver, memory-management circuitry, processor interface logic circuitry, and 64K × 16 bits of shared static random access memory. The memory is used to configure message and data blocks. In addition, 23 16-bit registers are available for (1) configuring the hybrid IC for, and starting it in, various modes of operation; (2) reading the status of the functionality of the hybrid IC; and (3) resetting the hybrid IC to a known state.



The miniBIC comprises, in effect, four MIL-STD-1553 interfaces that can operate independently or in coordination.

The miniBIC can operate as a remote terminal, bus controller, or bus monitor.

The FPGA provides the chip-select and data-strobe signals needed for operation of the hybrid ICs. The FPGA also receives interruption signals and forwards them to the ISA bus. The ISA interface connects the address, data, and control interfaces of the hybrid ICs to the ISA backplane.

Each channel is, in effect, a MIL-STD-1553 interface that can operate either

independently of the others or else as a redundant version of one of the others. The transformer in each channel provides electrical isolation between the rest of the miniBIC circuitry and the bus to which that channel is connected.

This work was done by Gary L. Cox of Johnson Space Center. For further information, contact the Johnson Commercial Technology Office at (281) 483-3809. MSC-23216

Improved Method of Locating Defects in Wiring Insulation

The best features of the DWV and TDR methods are combined.

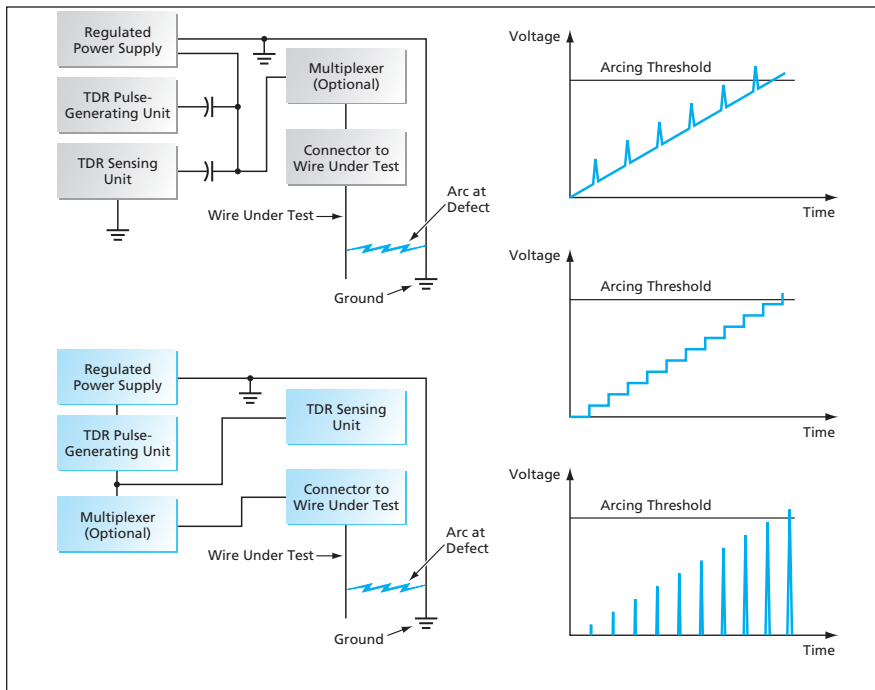
Ames Research Center, Moffett Field, California

An improved method of locating small breaches in insulation on electrical wires combines aspects of the prior dielectric withstand voltage (DWV) and time-domain reflectometry (TDR) methods. The

method was invented to satisfy a need for reliably and quickly locating insulation defects in spacecraft, aircraft, ships, and other complex systems that contain large amounts of wiring, much of it enclosed in

structures that make it difficult to inspect.

In the DWV method, one applies a predetermined potential (usually 1.5 kV DC) to the wiring and notes whether the voltage causes any arcing between the



A **Wire Is Tested** by applying a suitable voltage waveform to produce arcing and measuring the time between (1) the pulse or staircase edge that immediately precedes the arcing and (2) the receipt of the arcing signal at the location of application of the waveform. The distance to the defect where the arcing occurs is calculated from the time thus measured.

wiring and ground. The DWV method does not provide an indication of the location of the defect (unless, in an exceptional case, the arc happens to be visible). In addition, if there is no electrically conductive component at ground potential within about 0.010 in. (≈ 0.254 mm) of the wire at the location of an insulation defect, then the DWV method does not provide an indication of the defect. Moreover, one does not have the option to raise the potential in an effort to increase the detectability of such a defect because doing so can harm previously undamaged insulation.

In the TDR method as practiced heretofore, one applies a pulse of electricity having an amplitude of <25 V to a wire and measures the round-trip travel time for the reflection of the pulse from a defect. The distance along the wire from

the point of application of the pulse to the defect is then calculated as the product of half the round-trip travel time and the characteristic speed of a propagation of an electromagnetic signal in the wire. While the TDR method as practiced heretofore can be used to locate a short or open circuit, it does not ordinarily enable one to locate a small breach in insulation because the pulse voltage is too low to cause arcing and thus too low to induce an impedance discontinuity large enough to generate a measurable reflection.

The present improved method overcomes the weaknesses of both the prior DWV and the prior TDR method. One prepares the system to be tested by filling all or part of the system with a liquid or gas that does not harm the wiring and that is either electrically conductive or undergoes dielectric breakdown (and

thereby becomes electrically conductive) at a relatively low applied electric field. For example, if the system to be tested is an aircraft, one can fill the interior of the aircraft with neon, through which arcs can readily develop between wires and metal grounds. This permits arcing to a ground as far as 1.0 in. (≈ 25.4 mm) from the conductor.

The figure depicts two typical alternative assemblies of equipment that could be used to implement the present method, along with three typical alternative voltage waveforms that could be used in the method. Once the system to be tested has been prepared as described in the preceding paragraph, one of these waveforms is applied to a wire under test. In the case of the first waveform, one superimposes a conventional TDR signal on a gradually increasing voltage until arcing occurs. To make the arcing occur at the identifiable time of one of the TDR pulses (preventing the somewhat random arcing that might otherwise occur) and thereby make it possible to measure the round-trip travel time, (1) the rate of the interval between the TDR pulses is made long enough to encompass any reflections that might occur and (2) the rate of gradual increase of voltage is made such that highest voltage yet reached occurs at the peak of each superimposed TDR pulse.

The second voltage waveform is a staircase function. In this case, the highest voltage yet reached (and thus arcing) always occurs at a rising edge. The third waveform consists solely of TDR pulses, but unlike in conventional TDR, these are high-voltage pulses. In this case, the amplitude of the pulses is increased gradually until they cause arcing.

This work was done by Owen R. Greulich of Ames Research Center. Further information is contained in a TSP (see page 1).

Inquiries concerning rights for the commercial use of this invention should be addressed to the Patent Counsel, Ames Research Center, (650) 604-5104. Refer to ARC-14612.

Strobe Traffic Lights Warn of Approaching Emergency Vehicles

Simple, intuitive displays indicate directions of approach.

NASA's Jet Propulsion Laboratory, Pasadena, California

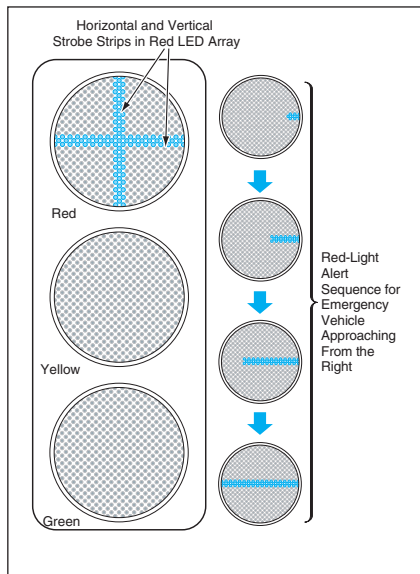
Strobe-enhanced traffic signals have been developed to aid in the preemption of road intersections for emergency vehicles. The strobe-enhanced traffic signals can be incorporated into both new

and pre-existing traffic-control systems in which the traffic-signal heads are of a relatively new type based on arrays of light-emitting diodes (LEDs). The strobe-enhanced traffic signals offer a

less expensive, less complex alternative to a recently developed system of LED-based warning signs placed next to traffic signals. Because of its visual complexity, the combination of traffic signals and

warning signs is potentially confusing to motorists. The strobe-enhanced traffic signals present less visual clutter.

In a given traffic-signal head, the strobe-enhanced traffic signal is em-



The LEDs in the Horizontal Strobe Strip are lit in sequence from right to left to indicate that an emergency vehicle is approaching from the right.

bedded in the red LED array of the “stop” signal. Two strobe LED strips — one horizontal and one vertical — are made capable of operating separately from the rest of the red LED matrix. When no emergency vehicle is approaching, the red LED array functions as a normal “stop” signal: all the red LEDs are turned on and off together. When the intersection is to be preempted for an approaching emergency vehicle, only the LEDs in one of the strobe strips are lit, and are turned on in a sequence that indicates the direction of approach. For example (see figure), if an emergency vehicle approaches from the right, the strobe LEDs are lit in a sequence moving from right to left.

Important to the success of strobe-enhanced traffic signals is conformance to city ordinances and close relation to pre-existing traffic standards. For instance, one key restriction is that new icons must not include arrows, so that motorists will not confuse new icons with conventional arrows that indicate allowed directions of movement. It is also critical that new displays like

strobe-enhanced traffic signals be similar to displays used in traffic-control systems in large cities. For example, Charleston, South Carolina uses horizontal strobes on red traffic lights to alert motorists and thereby help motorists not to miss red lights. The one significant potential disadvantage of strobe-enhanced traffic lights is initial unfamiliarity on the part of motorists.

This work was done by Aaron Bachelder of Caltech for NASA’s Jet Propulsion Laboratory. Further information is contained in a TSP (see page 1).

In accordance with Public Law 96-517, the contractor has elected to retain title to this invention. Inquiries concerning rights for its commercial use should be addressed to:

Intellectual Assets Office

JPL

Mail Stop 202-233

4800 Oak Grove Drive

Pasadena, CA 91109-8099

(818) 354-2240

E-mail: ipgroup@jpl.nasa.gov

Refer to NPO-30716, volume and number of this NASA Tech Briefs issue, and the page number.

Improved Timing Scheme for Spaceborne Precipitation Radar

This scheme enables automated targeting and prevents pulse collisions.

NASA’s Jet Propulsion Laboratory, Pasadena, California

An improved timing scheme has been conceived for operation of a scanning satellite-borne rain-measuring radar system. The scheme allows a real-time-generated solution, which is required for auto targeting. The current timing scheme used in radar satellites involves pre-computing a solution that allows the instrument to catch all transmitted pulses without transmitting and receiving at the same time. Satellite altitude requires many pulses in flight at any time, and the timing solution to prevent transmit and receive operations from colliding is usually found iteratively. The proposed satellite has a large number of scanning beams each with a different range to target and few pulses per beam. Furthermore, the satellite will be self-targeting, so the selection of which beams are used will change from sweep to sweep. The proposed timing solution guarantees no echo collisions, can be generated using simple FPGA-

based hardware in real time, and can be mathematically shown to deliver the maximum number of pulses per second, given the timing constraints.

The timing solution is computed every sweep, and consists of three phases: (1) a build-up phase, (2) a feedback phase, and (3) a build-down phase. Before the build-up phase can begin, the beams to be transmitted are sorted in numerical order. The numerical order of the beams is also the order from shortest range to longest range. Sorting the list guarantees no pulse collisions.

The build-up phase begins by transmitting the first pulse from the first beam on the list. Transmission of this pulse starts a delay counter, which stores the beam number and the time delay to the beginning of the receive window for that beam. The timing generator waits just long enough to complete the transmit pulse plus one re-

ceive window, then sends out the second pulse. The second pulse starts a second delay counter, which stores its beam number and time delay. This process continues until an output from the first timer indicates there is less than one transmit pulse width until the start of the next receive event. This blocks future transmit pulses in the build-up phase.

The feedback phase begins with the first timer paying off and starting the first receive window. When the first receive window is complete, the timing generator transmits the next beam from the list. When the second timer pays off, the second receive event is started. Following the second receive event, the timing generator will transmit the next beam on the list and start an additional timer. The timers work in a circular buffer fashion so there only need to be enough to cover the maximum number of echoes in flight.

When there are no more beams to transmit on the list, the build-down phase begins. In this phase, receive events begin when their respective timers pay off. When the timers have all paid off, the sweep is over and the instrument can begin a new sweep with a new list of beams.

Pulse collisions are avoided by the spacing of pulses during the build-up phase and by the order of the beams.

As long as the range (delay) never decreases there will always be enough time between any 2 transmit pulses for the receive window and it can occur at its optimal time. The solution is shown by simulation to average 90-percent efficiency in that the instrument is transmitting or receiving (but never both) 90 percent of the time. This can be shown to be optimal, given the constraint that the number of echoes in

flight needs to be constant over a sweep. This timing solution is the heart of an onboard processor/controller board for the second generation of Global Precipitation Mission.

The work is being done by Andrew Berkun and Mark Fischman of Caltech for NASA's Jet Propulsion Laboratory, with cooperation from consultant Ray Andraka. Further information is contained in a TSP (see page 1). NPO-30560

Concept for Multiple-Access Free-Space Laser Communications

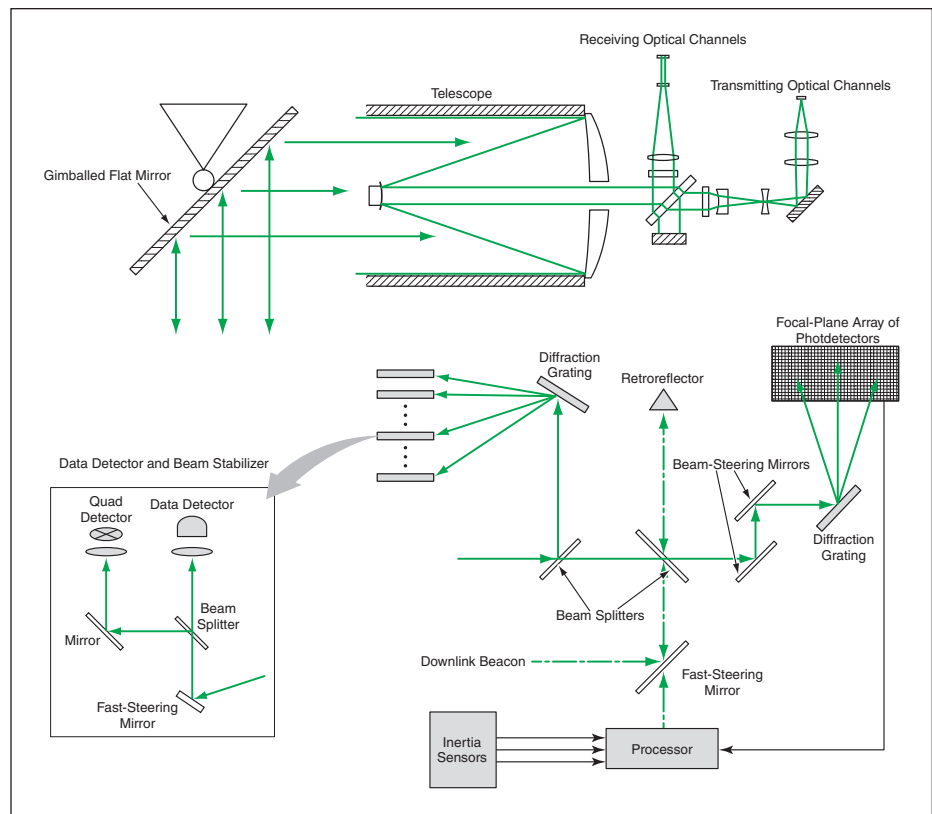
Multiple terminals at lower altitudes would be tracked by optomechanical and optoelectronic means.

NASA's Jet Propulsion Laboratory, Pasadena, California

A design concept for a proposed airborne or spaceborne free-space optical-communication terminal provides for simultaneous reception of signals from multiple other optical-communication terminals aboard aircraft or spacecraft that carry scientific instruments and fly at lower altitudes. The concept reflects the need for rapid acquisition and tracking of the signals coming from the lower-altitude terminals as they move across the field of view.

As shown in the upper part of the figure, the optical train of the terminal would include a telescope aimed at the scene below via a gimbaled flat mirror, which would be used to scan the field of view over a wide angular range. The lower part of the figure schematically depicts some of the optical and electronic channels used in the reception of data signals from, and the transmission of a beacon signal to, the lower terminals. This scheme is based on an architecture that provides for imaging of a small portion of the transmitted beam on a focal-plane array of photodetectors. Equipped with fast-read-out circuitry, the focal-plane array would be used in simultaneous acquisition and tracking.

The design concept includes an operational scenario in which each lower terminal would be assigned a unique uplink wavelength for its transmitted laser beam, which would serve as both its uplink communication beam and its beacon. An optical link would be initiated by a lower terminal, which would transmit a wide beam up to the higher terminal. The lower terminal would then await an



The **Optics and Electronics** in a higher optical-communication terminal would maintain communication with multiple lower terminals within its field of view.

acknowledgement of acquisition of its signal by the higher terminal before proceeding with a "handshake" and subsequent communications.

In the higher terminal, the uplinked beams from the lower terminals would be split between a data and a tracking channel, most of the beam power going to the data channel. In the tracking channel, the beams would then pass with minimal attenuation

through a dichroic beam splitter and onto two electronically actuated beam-steering mirrors, which would reflect the beams onto a diffraction grating that would separate the beams by wavelength. The beams would then impinge on separate spots on the focal-plane array of photodetectors.

The downlink beam would be reflected by a fast-steering mirror, which would be driven to correct for vibrations measured

by inertial sensors. The downlink beam would then be reflected out through the telescope by use of a mirror that would be partially (<1 percent) transmissive. The small part of the beacon beam transmitted through the mirror would impinge on a retroreflector and thereby be sent back to the focal-plane array to provide information on the pointing direction of the downlink beam.

The uplink from each lower terminal would be validated by means of the downlink beacon. To make this possible, the fast-steering mirror would also be made to rapidly scan the downlink beam across the locations of the lower termi-

nals as indicated by the locations of their beam spots on the focal-plane array.

In the data channel, the uplink signals would impinge on a diffraction grating, then each beam would be focused on data-detector-and-beam-stabilization unit (denoted in the figure as d_i for the i th beam). Each d_i would include a quadrant detector and a fine-steering mirror acting together as parts of a servo loop to maintain strength of the uplink signal on a data detector.

This work was done by Keith Wilson of Caltech for NASA's Jet Propulsion Laboratory. Further information is contained in a TSP (see page 1).

In accordance with Public Law 96-517, the contractor has elected to retain title to this invention. Inquiries concerning rights for its commercial use should be addressed to:

*Innovative Technology Assets Management
JPL*

*Mail Stop 202-233
4800 Oak Grove Drive
Pasadena, CA 91109-8099
(818) 354-2240*

E-mail: iaoffice@jpl.nasa.gov

Refer to NPO-30621, volume and number of this NASA Tech Briefs issue, and the page number.

Variable Shadow Screens for Imaging Optical Devices

Effective dynamic ranges would be increased.

Lyndon B. Johnson Space Center, Houston, Texas

Variable shadow screens have been proposed for reducing the apparent brightnesses of very bright light sources relative to other sources within the fields of view of diverse imaging optical devices, including video and film cameras and optical devices for imaging directly into the human eye. In other words, variable shadow screens would increase the effective dynamic ranges of such devices.

Traditionally, imaging sensors are protected against excessive brightness by use of dark filters and/or reduction of iris diameters. These traditional means do not increase dynamic range; they reduce the ability to view or image dimmer features of an image because they reduce the brightness of all parts of an image by the same factor. On the other hand, a variable shadow screen would darken only the excessively bright parts of an image. For example, dim objects in a field of view that included the setting Sun or bright headlights could be seen more readily in a picture taken through a variable shadow screen than in a picture of the same scene taken through a dark filter or a narrowed iris.

The figure depicts one of many potential variations of the basic concept of the variable shadow screen. The shadow screen would be a normally transparent liquid-crystal matrix placed in front of a focal-plane array of photodetectors in a charge-coupled-device

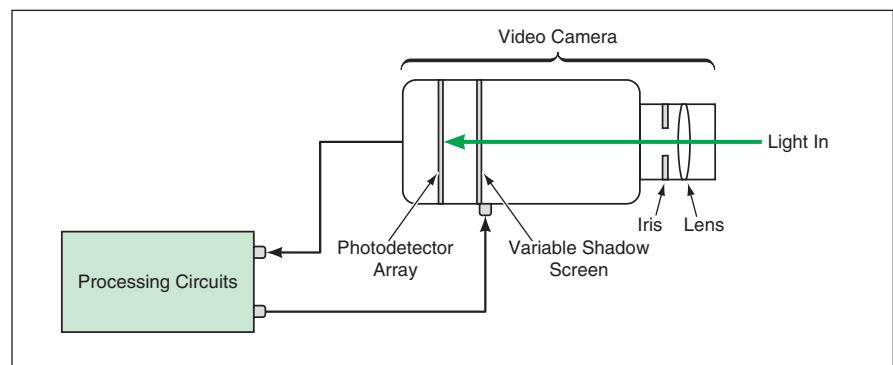


Image Feedback From the Focal Plane would be processed to generate a thresholded negative image on the shadow plane.

video camera. The shadow screen would be placed far enough from the focal plane so as not to disrupt the focal-plane image to an unacceptable degree, yet close enough so that the out-of-focus shadows cast by the screen would still be effective in darkening the brightest parts of the image.

The image detected by the photodetector array itself would be used as feedback to drive the variable shadow screen: The video output of the camera would be processed by suitable analog and/or digital electronic circuitry to generate a negative partial version of the image to be impressed on the shadow screen. The parts of the shadow screen in front of those parts of the image with brightness below a specified threshold would be left

transparent; the parts of the shadow screen in front of those parts of the image where the brightness exceeded the threshold would be darkened by an amount that would increase with the excess above the threshold.

This work was done by Ed Lu of Johnson Space Center and Jean L. Chretien (an independent contributor). For further information, contact the Johnson Commercial Technology Office at (281) 483-3809.

This invention is owned by NASA, and a patent application has been filed. Inquiries concerning nonexclusive or exclusive license for its commercial development should be addressed to the Patent Counsel, Johnson Space Center, (281) 483-0837. Refer to MSC-23037.

☒ Verifying Diagnostic Software

Livingstone PathFinder (LPF) is a simulation-based computer program for verifying autonomous diagnostic software. LPF is designed especially to be applied to NASA's Livingstone computer program, which implements a qualitative-model-based algorithm that diagnoses faults in a complex automated system (e.g., an exploratory robot, spacecraft, or aircraft). LPF forms a software test bed containing a Livingstone diagnosis engine, embedded in a simulated operating environment consisting of a simulator of the system to be diagnosed by Livingstone and a driver program that issues commands and faults according to a non-deterministic scenario provided by the user. LPF runs the test bed through all executions allowed by the scenario, checking for various selectable error conditions after each step. All components of the test bed are instrumented, so that execution can be single-stepped both backward and forward. The architecture of LPF is modular and includes generic interfaces to facilitate substitution of alternative versions of its different parts. Altogether, LPF provides a flexible, extensible framework for simulation-based analysis of diagnostic software; these characteristics also render it amenable to application to diagnostic programs other than Livingstone.

This program was written by Tony Lindsey and Charles Pecheur of Ames Research Center. Further information is contained in a TSP (see page 1).

Inquiries concerning rights for the commercial use of this invention should be addressed to the Patent Counsel, Ames Research Center, (650) 604-5104. Refer to ARC-14780-1.

☒ Initial Processing of Infrared Spectral Data

The Atmospheric Infrared Spectrometer (AIRS) Science Processing System is a collection of computer programs, denoted product generation executives (PGEs), for processing the readings of the AIRS suite of infrared and microwave instruments orbiting the Earth aboard NASA's Aqua spacecraft. Following from level 0 (representing raw AIRS data), the PGEs and their data products are denoted by alphanumeric labels

(1A, 1B, and 2) that signify the successive stages of processing. Once level-0 data have been received, the level-1A PGEs begin processing, performing such basic housekeeping tasks as ensuring that all the Level-0 data are present and ordering the data according to observation times. The level-1A PGEs then perform geolocation-refinement calculations and conversions of raw data numbers to engineering units. Finally, the level-1A data are grouped into packages, denoted granules, each of which contain the data from a six-minute observation period. The granules are forwarded, along with calibration data, to the Level-1B PGEs for processing into calibrated, geolocated radiance products. The Level-2 PGEs, which are not yet operational, are intended to process the level-1B data into temperature and humidity profiles, and other geophysical properties.

This program was written by Solomon De Picciotto, Albert Chang, Zi-Ping Sun, Yuan-Ti Ting, Evan Manning, Steven Gaiser, Bjorn Lambriksen, Mark Hofstadter, Thomas Hearty, Thomas Pagano, Hartmut Aumann, and Steven Broberg of Caltech for NASA's Jet Propulsion Laboratory. Further information is contained in a TSP (see page 1).

This software is available for commercial licensing. Please contact Don Hart of the California Institute of Technology at (818) 393-3425. Refer to NPO-35243.

☒ Activity-Centric Approach to Distributed Programming

The first phase of an effort to develop a NASA version of the Cybele software system has been completed. To give meaning to even a highly abbreviated summary of the modifications to be embodied in the NASA version, it is necessary to present the following background information on Cybele:

Cybele is a proprietary software infrastructure for use by programmers in developing agent-based application programs [complex application programs that contain autonomous, interacting components (agents)]. Cybele provides support for event handling from multiple sources, multithreading, concurrency control, migration, and load balancing. A Cybele agent follows a programming paradigm, called activity-centric programming, that enables an abstraction over system-level thread mechanisms. Activity-

centric programming relieves application programmers of the complex tasks of thread management, concurrency control, and event management. In order to provide such functionality, activity-centric programming demands support of other layers of software. This concludes the background information.

In the first phase of the present development, a new architecture for Cybele was defined. In this architecture, Cybele follows a modular service-based approach to coupling of the programming and service layers of software architecture. In a service-based approach, the functionalities supported by activity-centric programming are apporportioned, according to their characteristics, among several groups called services. A well-defined interface among all such services serves as a path that facilitates the maintenance and enhancement of such services without adverse effect on the whole software framework. The activity-centric application-program interface (API) is part of a kernel. The kernel API calls the services by use of their published interface. This approach makes it possible for any application code written exclusively under the API to be portable for any configuration of Cybele.

This program was written by Renato Levy, Goutam Satapathy, and Jun Lang of Intelligent Automation, Inc., for Johnson Space Center. For further information, contact:

*Intelligent Automation, Inc.
2 Research Place, Suite 202
Rockville, MD 20850
Refer to MSC-23239.*

☒ Controlling Distributed Planning

A system of software implements an extended version of an approach, denoted shared activity coordination (SHAC), to the interleaving of planning and the exchange of plan information among organizations devoted to different missions that normally communicate infrequently except that they need to collaborate on joint activities and/or the use of shared resources. SHAC enables the planning and scheduling systems of the organizations to coordinate by resolving conflicts while optimizing local planning solutions. The present software provides a framework for modeling and executing communication

protocols for SHAC. Shared activities are represented in each interacting planning system to establish consensus on joint activities or to inform the other systems of consumption of a common resource or a change in a shared state. The representations of shared activities are extended to include information on (1) the role(s) of each participant, (2)

permissions (defined as specifications of which participant controls what aspects of shared activities and scheduling thereof), and (3) constraints on the parameters of shared activities. Also defined in the software are protocols for changing roles, permissions, and constraints during the course of coordination and execution.

*This program was written by Bradley Clement and Anthony Barrett of Caltech for **NASA's Jet Propulsion Laboratory**. Further information is contained in a TSP (see page 1).*

This software is available for commercial licensing. Please contact Don Hart of the California Institute of Technology at (818) 393-3425. Refer to NPO-40438



New Material for Surface-Enhanced Raman Spectroscopy

Reproducible measurements can be made quickly, without preparation of samples.

Lyndon B. Johnson Space Center, Houston, Texas

A chemical method of synthesis and application of coating materials that are especially suitable for surface-enhanced Raman spectroscopy (SERS) has been developed. The purpose of this development is to facilitate the utilization of the inherently high sensitivity of SERS to detect chemicals of interest (analytes) in trace amounts, without need for lengthy sample preparation.

Up to now, the use of SERS has not become routine because the methods available have not been able to reproduce sampling conditions and provide quantitative measurements. In contrast, the coating materials of the present method enable analysis with minimum preparation of samples, and SERS measurements made using these materials are reproducible and reversible. Moreover, unlike in methods investigated in prior efforts to implement SERS, sampling is not restricted to such specific environments as electrolytes or specific solvents.

The coating materials of this method are porous glasses, formed in sol-gel processes, that contain small particles of gold or silver metal. Materials of this type can be applied to the sample-contact surfaces of a variety of sampling and sensing devices, including glass slides, glass vials, fiber-optic probes, and glass tubes. Glass vials with their in-

teriors coated according to this method are particularly convenient for SERS to detect trace chemicals in solutions: One simply puts a sample solution containing the analyte(s) into a vial, then puts the vial into a Raman spectrometer for analysis.

The chemical ingredients and the physical conditions of the sol-gel process have been selected so that the porous glass formed incorporates particles of the desired metal with size(s) to match the wavelength(s) of the SERS excitation laser in order to optimize the generation of surface plasmons. The ingredients and processing conditions have further been chosen to tailor the porosity and polarity of the glass to optimize the sample flow and the interaction between the analyte(s) and the plasmon field that generates Raman photons.

The porous silica network of a sol-gel glass creates a unique environment for stabilizing SERS-active metal particles. Relative to other material structures that could be considered for SERS, the porous silica network offers higher specific surface area and thus greater interaction between analyte molecules and metal particles.

Efforts to perform SERS measurements with the help of sampling devices

coated by this method have been successful. In tests, numerous organic and inorganic chemicals were analyzed in several solvents, including water. The results of the tests indicate that the SERS measurements were reproducible within 10 percent and linear over five orders of magnitude. One measure of the limits of detectability of chemicals in these tests was found to be a concentration of 300 parts per billion. Further development may eventually make it possible to realize the full potential sensitivity of SERS for detecting some analytes in quantities as small as a single molecule.

This work was done by Stuart Farquharson, Chad Nelson, and Yuan Lee of Advanced Fuels Research Inc. for Johnson Space Center.

In accordance with Public Law 96-517, the contractor has elected to retain title to this invention. Inquiries concerning rights for its commercial use should be addressed to:

*Advanced Fuel Research, Inc.
87 Church Street
East Hartford, CT 06108
Telephone No.: (860) 528-9806
Fax No.: (860) 528-0648
Internet: info@AFRinc.com*

Refer to MSC-23197, volume and number of this NASA Tech Briefs issue, and the page number.

Treated Carbon Nanofibers for Storing Energy in Aqueous KOH

Treatment can increase specific capacitance by as much as 400 percent.

Lyndon B. Johnson Space Center, Houston, Texas

A surface treatment has been found to enhance the performances of carbon nanofibers as electrode materials for electrochemical capacitors in which aqueous solutions of potassium hydroxide are used as the electrolytes. In the treatment, sulfonic acid groups are attached to edge plane sites on carbon atoms.

The treatment is applicable to a variety of carbon nanofibers, including fib-

ers and both single- and multiple-wall nanotubes. The reason for choosing nanofibers over powders and other forms of carbon is that nanofibers offer greater power features.

In previous research, it was found that the surface treatment of carbon nanofibers increased energy-storage densities in the presence of acid electrolytes. Now, it has been found that the same treatment increases energy-

storage densities of carbon nanofibers in the presence of alkaline electrolytes when the carbon is paired with a NiOOH electrode. This beneficial effect varies depending on the variety of carbon substrate to which it is applied.

It has been conjectured that the sulfonic acid groups, which exist in a deprotonated state in aqueous KOH solutions, undergo reversible electro-

chemical reactions that are responsible for the observed increases in energy-storage capacities. The increases can be considerable: For example, in one case, nanofibers exhibited a specific capacitance of 34 Farads per gram before treatment and 172 Farads per gram (an increase of about 400 percent) after treatment.

The most promising application of this development appears to lie in hybrid capacitors, which are devices designed primarily for storing energy. These devices are designed to be capable of (1) discharge at rates greater

than those of batteries and (2) storing energy at densities approaching those of batteries. A hybrid capacitor includes one electrode like that of a battery and one electrode like that of an electrochemical capacitor. For example, a hybrid capacitor could contain a potassium hydroxide solution as the electrolyte, a carbon capacitor electrode, and a nickel hydroxide battery electrode. By making the capacitor electrode of treated carbon nanofibers instead of another carbon material, one could obtain greater energy-storage capacity.

This work was done by David W. Firsich of Inorganic Specialists, Inc. for Johnson Space Center.

In accordance with Public Law 96-517, the contractor has elected to retain title to this invention. Inquiries concerning rights for its commercial use should be addressed to:

Inorganic Specialists, Inc.

720 Mound Ave.

Miamisburg, OH 45343-0181

Refer to MSC-23321, volume and number of this NASA Tech Briefs issue, and the page number.



Advanced Infant Car Seat Would Increase Highway Safety

This system would keep a baby safe, comfortable, and entertained, thereby reducing distractions for an adult driver.

Marshall Space Flight Center, Alabama

An advanced infant car seat has been proposed to increase highway safety by reducing the incidence of crying, fussy behavior, and other child-related distractions that divert an adult driver's attention from driving. In addition to a conventional infant car seat

with safety restraints, the proposed advanced infant car seat would include a number of components and subsystems that would function together as a comprehensive infant-care system that would keep its occupant safe, comfortable, and entertained, and would en-

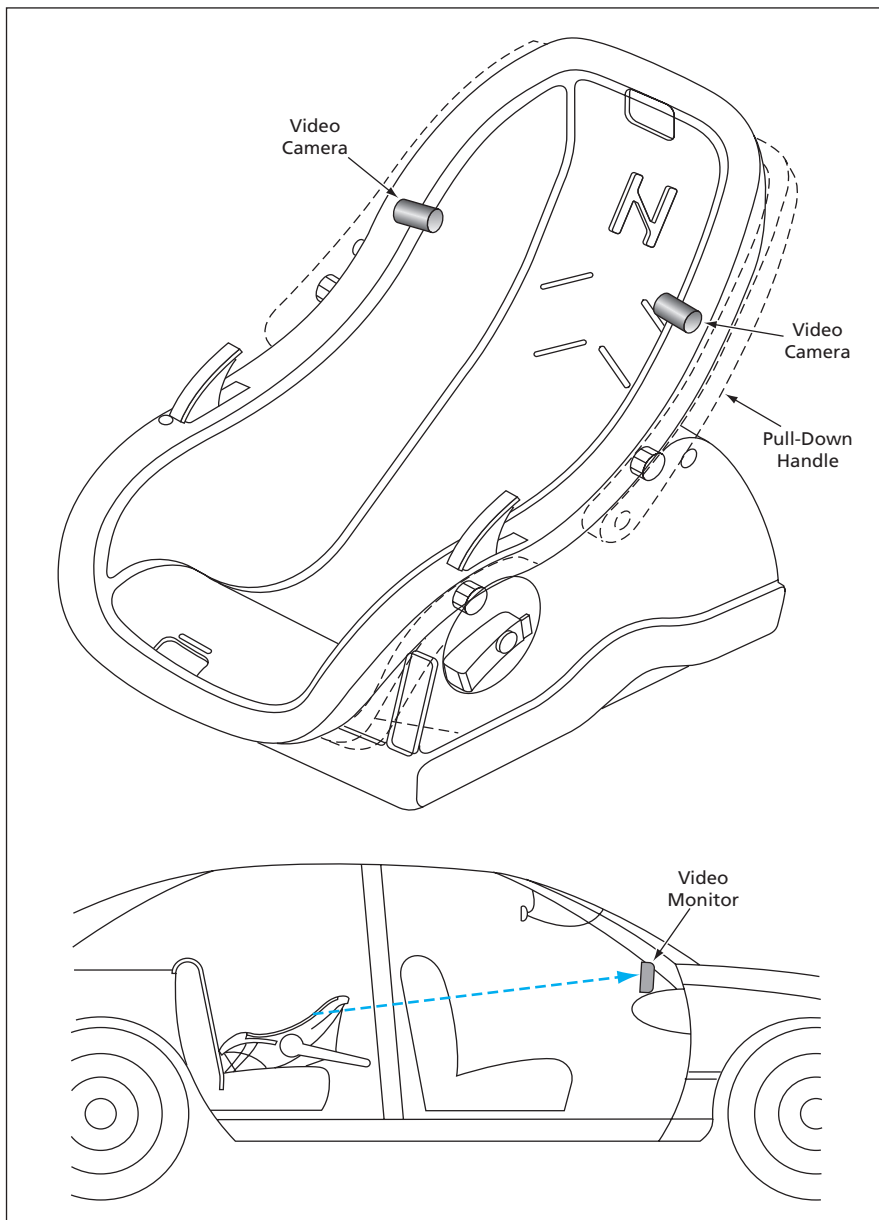
able the driver to monitor the baby without having to either stop the car or turn around to face the infant during driving.

The system would include a vibrator with bulb switch to operate; the switch would double as a squeeze toy that would make its own specific sound. A music subsystem would include loudspeakers built into the seat plus digital and analog circuitry that would utilize plug-in memory modules to synthesize music or a variety of other sounds. The music subsystem would include a built-in sound generator that could synthesize white noise or a human heartbeat to calm the baby to sleep. A second bulb switch could be used to control the music subsystem and would double as a squeeze toy that would make a distinct sound.

An antinoise sound-suppression system would isolate the baby from potentially disturbing ambient external noises. This subsystem would include small microphones, placed near the baby's ears, to detect ambient noise. The outputs of the microphone would be amplified and fed to the loudspeakers at appropriate amplitude and in a phase opposite that of the detected ambient noise, such that the net ambient sound arriving at the baby's ears would be almost completely cancelled.

A video-camera subsystem would enable the driver to monitor the baby visually while continuing to face forward. One or more portable miniature video cameras could be embedded in the side of the infant car seat (see figure) or in a flip-down handle. The outputs of the video cameras would be transmitted by radio or infrared to a portable, miniature receiver/video monitor unit that would be attached to the dashboard of the car. The video-camera subsystem can also be used within transmission/reception range when the seat was removed from the car.

The system would include a biotelemetric and tracking subsystem, which would include a Global Positioning System receiver for measuring its location.



Miniature Video Cameras in the sides of the advanced infant car seat would transmit images to a video monitor on the dashboard, enabling the driver to monitor the infant visually while facing the road ahead.

This subsystem would transmit the location of the infant car seat (even if the seat were not in a car) along with such biometric data as the baby's heart rate, perspiration rate, urinary status, temperature, and rate of breathing. Upon detecting any anomalies in the biometric data, this subsystem would send a warning to a paging device installed in the car or carried by the driver, so that the driver could pull the car off the road to attend to the baby. A motion detector in

this subsystem would send a warning if the infant car seat were to be moved or otherwise disturbed unexpectedly while the infant was seated in it: this warning function, in combination with the position-tracking function, could help in finding a baby who had been kidnapped with the seat.

Removable rechargeable batteries would enable uninterrupted functioning of all parts of the system while transporting the baby to and from the car.

The batteries could be recharged via the cigarette-lighter outlet in the car or by use of an external AC-powered charger.

*This work was done by Richard Dabney and Susan Elrod of **Marshall Space Flight Center**.*

This invention is owned by NASA, and a patent application has been filed. For further information, contact Sammy Nabors, MSFC Commercialization Assistance Lead, at sammy.a.nabors@nasa.gov. Refer to MFS-31707-1/8/14-1.



Development of Biomorphic Flyers

Autonomous flight control and navigation in small size is offered for planetary and terrestrial exploration applications.

NASA's Jet Propulsion Laboratory, Pasadena, California

Biomorphic flyers have recently been demonstrated that utilize the approach described earlier in "Bio-Inspired Engineering of Exploration Systems" (NPO-21142), *NASA Tech Briefs*, Vol. 27, No. 5 (May 2003), page 54, to distill the principles found in successful, nature-tested mechanisms of flight control. Two types of flyers are being built, corresponding to the imaging and shepherding flyers for a biomorphic mission described earlier in "Cooperative Lander-Surface/Aerial Microflyer Missions for Mars Exploration" (NPO-30286), *NASA Tech Briefs*, Vol. 28, No. 5 (May 2004), page 36. The common features of these two types of flyers are that both are delta-wing airplanes incorporating bio-inspired capabilities of control, navigation, and visual search for exploration. The delta-wing design is robust to ~40 G axial load and offers ease of stowing and packaging.

The prototype that we have built recently is shown in the figure. Such levels of miniaturization and autonomous navigation are essential to enable biomorphic microflyers (<1 kg) that can be deployed in large numbers for distributed measurements and exploration of difficult terrain while avoiding hazards. Individual bio-inspired sensors that will be incorporated in a biomorphic flyer have been demonstrated recently. These sensors include a robust, lightweight (~6 g), and low-power (~40 mW) horizon sensor for flight stabilization. It integrates success-

fully the principles of the dragonfly ocelli. The ocelli are small eyes on the dorsal and forward regions of the heads of many insects. The ocelli are distinct from the compound eyes that are most commonly associated with insect vision. In many insects, the ocelli are little more than single-point detectors of short-wavelength light and behavioral responses to ocelli stimuli are hard to observe. The notable exception is found in dragonflies, where flight control is notably degraded by any interference with the ocellar system. Our team has discovered recently that the ocelli are a dedicated horizon sensor, with substantial optical processing and multiple spectral sensitivity. To our knowledge, this is the world's first demonstrated use of a "biomorphic ocellus" as a flight-stabilization system.

The advantage of the ocelli over a similarly sized system of rate gyroscopes is

that both attitude control and rate damping can be realized in one device. A full inertial unit and significant processing would otherwise be required to achieve the same effect. As a prelude to full autonomy, substantial stability augmentation is provided to the pilot at very low cost in terms of space, power, and mass. The sensor is about 40 times lighter than a comparable inertial attitude reference system. Other significant features of the biomorphic flyer shown in the figure include its ability to fly at high angles of attack ~30° and a deep wing chord which allows scaling to small size and low Reynold's number situations. Furthermore, the placement of the propulsion system near the center of gravity allows continued control authority at low speeds. These attributes make such biomorphic flyers uniquely suited to planetary and terrestrial exploration where small size and autonomous airborne operation are required.

This work was done by Sarita Thakoor of Caltech for NASA's Jet Propulsion Laboratory and by Dean Soccol, G. Stange, Geno Ewyk, Matt Garratt, M. Srinivasan, and Javaan Chahl of Australian National University and Butler Hine and Steven Zornetzer of Ames Research Center for the NASA Intelligent Systems Program. Automated Precision, Inc. Further information is contained in a TSP (see page 1).

NPO-30554



Photograph shows the **Biomorphic Flyer Platform**. The platform was successfully demonstrated in 2001.

Second-Generation Six-Limbed Experimental Robot

This robot is designed to be more agile and dexterous than its predecessor.

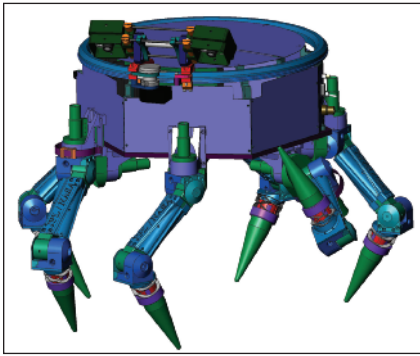
NASA's Jet Propulsion Laboratory, Pasadena, California

The figure shows the LEMUR II — the second generation of the Limbed Excursion Mechanical Utility Robot (LEMUR), which was described in "Six-Legged Experimental Robot" (NPO-20897), *NASA Tech Briefs*, Vol. 25, No. 12 (December 2001), page 58. The LEMUR II incorporates a number of improvements, including new features, that extend its capabili-

ties beyond those of its predecessor, which is now denoted the LEMUR I.

To recapitulate: the LEMUR I was a six-limbed robot for demonstrating robotic capabilities for assembly, maintenance, and inspection. The LEMUR I was designed to be capable of walking autonomously along a truss structure toward a mechanical assembly at a

prescribed location and to perform other operations. The LEMUR I was equipped with stereoscopic video cameras and image-data-processing circuitry for navigation and mechanical operations. It was also equipped with a wireless modem, through which it could be commanded remotely. Upon arrival at a mechanical assembly, the LEMUR I would perform



The LEMUR II can move its stereoscopic cameras along a circular track to view objects at any azimuth. Its symmetrical arrangement of six limbs enables motion along any azimuth heading.

simple mechanical operations with one or both of its front limbs. It could also transmit images to a host computer.

Each of the six limbs of the LEMUR I was operated independently. Each of the four rear limbs had three degrees of freedom (DOFs), while each of the front two limbs had four DOFs. The front two limbs were designed to hold, operate, and/or be integrated with tools. The LEMUR I included an onboard computer equipped with an assortment of digital control circuits, digital input/output circuits, analog-to-digital converters

for input, and digital-to-analog (D/A) converters for output. Feedback from optical encoders in the limb actuators was utilized for closed-loop microcomputer control of the positions and velocities of the actuators.

The LEMUR II incorporates the following improvements over the LEMUR I:

- The drive trains for the joints of the LEMUR II are more sophisticated, providing greater torque and accuracy.
- The six limbs are arranged symmetrically about a hexagonal body platform instead of in straight lines along the sides. This symmetrical arrangement is more conducive to omnidirectional movement in a plane.
- The number of degrees of freedom of each of the rear four limbs has been increased by one. Now, every limb has four degrees of freedom: three at the hip (or shoulder, depending on one's perspective) and one at the knee (or elbow, depending on one's perspective).
- Now every limb (instead of only the two front limbs) can perform operations. For this purpose, each limb is tipped with an improved quick-release mechanism for swapping of end-effector tools.
- New end-effector tools have been developed. These include an instrumented

rotary driver that accepts all tool bits that have 0.125-in. (3.175-mm)-diameter shanks, a charge-coupled-device video camera, a super bright light-emitting diode for illuminating the work area of the robot, and a generic collet tool that can be quickly and inexpensively modified to accept any cylindrical object up to 0.5 in. (12.7 mm) in diameter.

- The stereoscopic cameras are mounted on a carriage that moves along a circular track, thereby providing for omnidirectional machine vision.
- The control software has been augmented with software that implements innovations reported in two prior NASA *Tech Briefs* articles: the HIPS algorithm ["Hybrid Image-Plane/Stereo Manipulation" (NPO-30492), Vol. 28, No. 7 (July 2004), page 55] and the CAMPOUT architecture ["An Architecture for Controlling Multiple Robots" (NPO-30345), Vol. 28, No. 10 (October 2004), page 65].

This work was done by Brett Kennedy, Avi Okon, Hrand Aghazarian, Matthew Robinson, Michael Garrett, and Lee Magnone of Caltech for NASA's Jet Propulsion Laboratory. Further information is contained in a TSP (see page 1). NPO-35140

⚙️ Miniature Linear Actuator for Small Spacecraft

Goddard Space Flight Center, Greenbelt, Maryland

A report discusses the development of a kit of mechanisms intended for use aboard future spacecraft having masses between 10 and 100 kg. The report focuses mostly on two prototypes of one of the mechanisms: a miniature linear actuator based on a shape-memory-alloy (SMA) wire. In this actuator, as in SMA-wire actuators described previously in *NASA Tech Briefs*, a spring biases a moving part toward one limit of its stroke and is restrained or pulled toward the other limit of the stroke by an SMA wire, which as-

sumes a slightly lesser or greater "remembered" length, depending on whether or not an electric current is applied to the wire to heat it above a transition temperature. Topics addressed in the report include the need to develop mechanisms like these, the general approach to be taken in designing SMA actuators, tests of the two prototypes of the miniature linear actuators, and improvements in the second prototype over the first prototype resulting in reduced mass and increased stroke. The report also presents recom-

mendations for future development, briefly discusses problems of tolerances and working with small parts, states a need for better understanding of behaviors of SMAs, and presents conclusions.

This work was done by Cliff E. Willey and Stuart W. Hill of Johns Hopkins University Applied Physics Laboratory for Goddard Space Flight Center. Further information is contained in a TSP (see page 1). GSC-14706-1

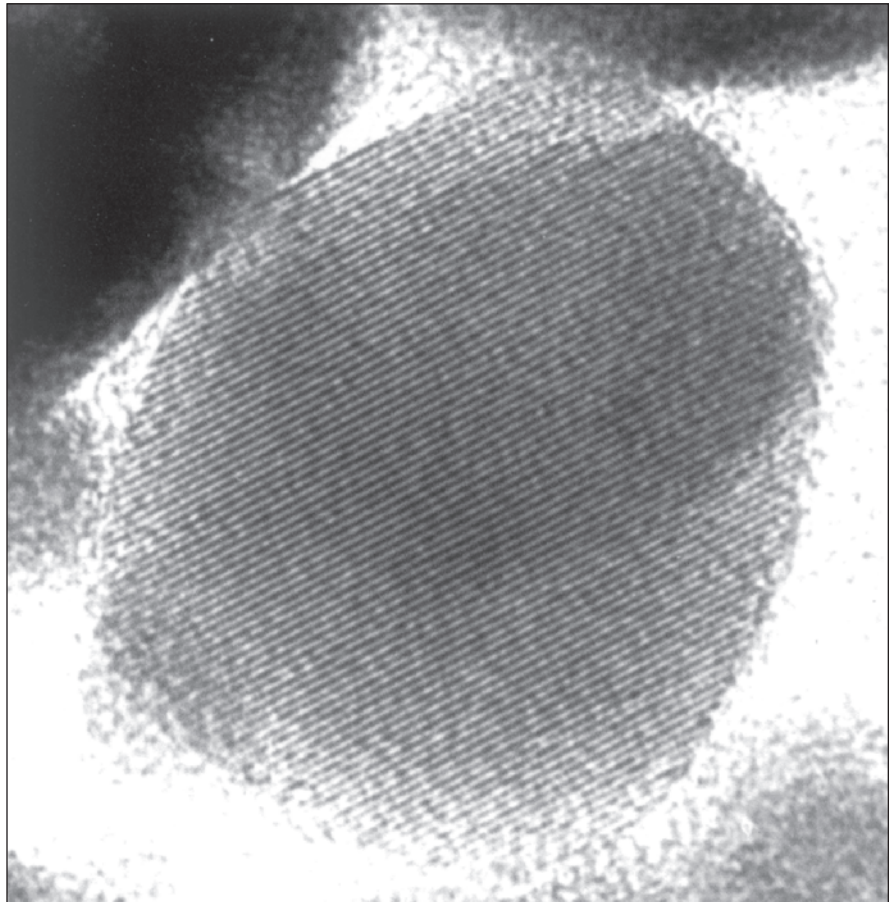
Process for Making Single-Domain Magnetite Crystals

Crystals can be chemically pure and free of defects.

Lyndon B. Johnson Space Center, Houston, Texas

A process for making chemically pure, single-domain magnetite crystals substantially free of structural defects has been invented as a byproduct of research into the origin of globules in a meteorite found in Antarctica and believed to have originated on Mars. The globules in the meteorite comprise layers of mixed (Mg, Fe, and Ca) carbonates, magnetite, and iron sulfides. Since the discovery of the meteorite was announced in August 1996, scientists have debated whether the globules are of biological origin or were formed from inorganic materials by processes that could have taken place on Mars. While the research that led to the present invention has not provided a definitive conclusion concerning the origin of the globules, it has shown that globules of a different but related chemically layered structure can be grown from inorganic ingredients in a multistep precipitation process. As described in more detail below, the present invention comprises the multistep precipitation process plus a subsequent heat treatment.

The multistep precipitation process was demonstrated in a laboratory experiment on the growth of submicron ankerite crystals, overgrown by submicron siderite and pyrite crystals, overgrown by submicron magnesite crystals, overgrown by submicron siderite and pyrite. In each step, chloride salts of appropriate cations (Ca, Fe, and Mg) were dissolved in deoxygenated, CO₂-saturated water. NaHCO₃ was added as a pH buffer while CO₂ was passed continuously through the solution. A 15-mL aliquot of the resulting solution was transferred into each of several 20 mL, poly(tetrafluoroethylene)-lined hydrothermal pressure vessels. The vessels were closed in a CO₂ atmosphere, then transferred into an oven at a temperature of 150 °C. After a predetermined time, the hydrothermal vessels were removed from the oven and quenched in a freezer. Supernatant solutions were decanted, and carbonate precipitates were washed free of soluble salts by repeated decantations with deionized water.



This **Transmission Electron Micrograph** shows a defect-free magnetite crystal with a (111) orientation, produced by thermal decomposition of siderite. The lattice fringes are spaced at 4.8 Å.

The procedure as described thus far was repeated for each subsequent step, except that a chemically different solution was added to the washed carbonate precipitates left in the hydrothermal vessels from the previous steps. Sulfur was included in the second and fourth steps to form Fe sulfides in addition to siderite. Hence, each globule comprised an ankeritic core (formed in step 1) followed by concentric zones of siderite + pyrite (formed in step 2), magnesite (formed in step 3), and siderite + pyrite (formed in step 4).

The carbonate + pyrite globules thus synthesized were heated to, then cooled from, 470 °C in a differential scanning calorimeter at the rate of 20 °C/min in a stream of CO₂ at a pressure of 13.3 kPa.

This heat treatment converted the siderite + pyrite to magnetite + pyrrhotite. The magnetite crystals are believed to have formed from the thermal decomposition of the siderite crystals in the reaction $3\text{FeCO}_3 \rightarrow \text{Fe}_3\text{O}_4 + 2\text{CO}_2 + \text{CO}$. The magnetite crystals were found to have a variety of shapes, to have linear dimensions of predominantly 10 to 100 nm (in the superparamagnetic-to-single-domain size range), to be chemically pure, and to be free of structural defects (see figure).

Magnetite powders are essential ingredients of magnetic recording tapes. Powders made from single-domain magnetite crystals may enable the production of magnetic tapes capable of storing data at densities greater than

are now possible, provided that the process can be refined so that the magnetite globules are mostly elongated along their (111) crystallographic axes. At the time of reporting the information for this article, scanning-electron-microscopy and electron-diffraction experiments to determine length-to-width

ratios and crystallographic orientations were under way.

This work was done by D. C. Golden of Hernandez Engineering; Douglas W. Ming, Richard V. Morris, Gary E. Lofgren, and Gordon A. McKay of Johnson Space Center; and Craig S. Schwandt, Howard V. Lauer, Jr., and Richard A. Socki of Lockheed Martin.

This invention is owned by NASA, and a patent application has been filed. Inquiries concerning nonexclusive or exclusive license for its commercial development should be addressed to the Patent Counsel, Johnson Space Center, (281) 483-0837. Refer to MSC-23326.

A New Process for Fabricating Random Silicon Nanotips

This process is relatively simple and inexpensive.

NASA's Jet Propulsion Laboratory, Pasadena, California

An improved process for the fabrication of random arrays of silicon nanotips has been demonstrated to be feasible. Relative to other such processes, this process offers advantages of low cost and simplicity. Moreover, this process can readily be combined with other processes used to fabricate integrated circuits and other monolithic silicon structures.

Arrays of silicon nanotips are subjects of research and development efforts directed toward utilizing them as field emitters in flat-panel displays, vacuum microelectronics, and microwave devices. Other silicon-nanotip-fabrication processes developed thus far predominantly include lithography, etching, and/or elaborate deposition steps followed by oxide sharpening steps and are both process intensive as well as expensive. In addition to being cheaper and simpler, the present process can efficiently produce silicon nanotips that range in height from a few microns to several tens of microns and are distributed over large areas.

The process mentioned here can be summarized as consisting of (1) the growth of micro-etch masks on a silicon substrate, followed by (2) etching away of the masks, along with some of the substrate, to make an array of sharp tips. In the first step of the process, a cleaned silicon substrate is subjected to reactive ion etching (RIE) in a certain mixture of oxygen and carbon tetrafluoride under radio-frequency excitation. This process step results in the growth of fluorine based compounds in the form of stumps randomly distributed

on the substrate. These stumps are known in the art as "polymer RIE grass." The dimensions of these stumps are of the order of hundreds of nanometers, the exact values depending on process time and gas composition. The areal density of the stumps decreases with increasing process time as they grow and merge with neighboring stumps. These stumps constitute the micro-etch masks for the next step of the process.

In the second step of the process, the substrate covered with the micro-etch masks is subjected to deep reactive ion etching (DRIE) process, which consists of cycles of reactive ion etching alternating with passivation (the Bosch process). The gas used in the etching substeps is sulfur hexafluoride (SF_6); the gas used in the passivation substeps is octafluorocyclobutane (C_4F_8). The portions of the substrate directly under the RIE grass stumps are etched more slowly than are the portions between the stumps. Hence, what remains at the end of the process, after the stumps and parts of the substrate have been etched away,

are silicon spikes where the stubs were (see figure).

In a variation of the process, one starts with a silicon or silicon-on-insulator substrate with the intent to etch through the full thickness of the substrate. That is to say, one chooses the thickness so that the DRIE step releases individual nanotips. Such individual silicon nanotips may have utility as microscopic probes in biomedical applications.

This work was done by Harish Manohara of Caltech for NASA's Jet Propulsion Laboratory. Further information is contained in a TSP (see page 1).

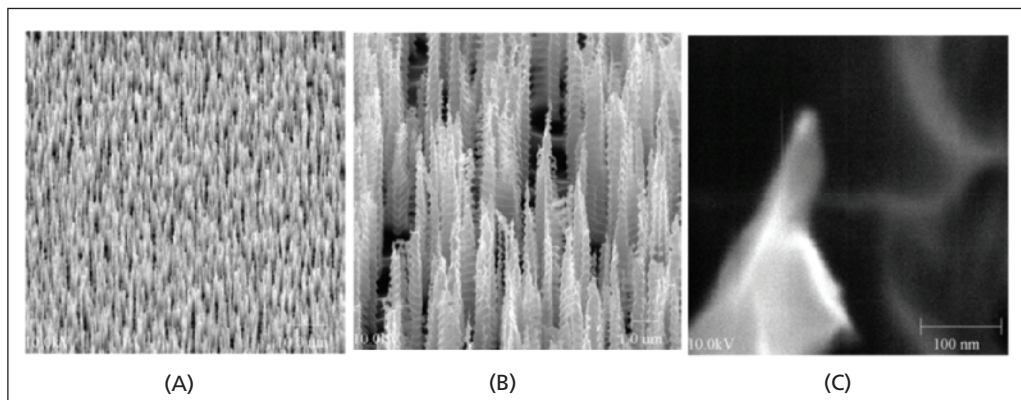
In accordance with Public Law 96-517, the contractor has elected to retain title to this invention. Inquiries concerning rights for its commercial use should be addressed to:

*Innovative Technology Assets Management
JPL*

*Mail Stop 202-233
4800 Oak Grove Drive
Pasadena, CA 91109-8099
(818) 354-2240*

E-mail: iaoffice@jpl.nasa.gov

Refer to NPO-40123, volume and number of this NASA Tech Briefs issue, and the page number.



An Array of Silicon Nanotips, shown here at three different magnifications, was fabricated as described in the text. The heights of these nanotips range from about 5 to about 6 μm . The average diameter of the sharp tip portions is about 20 nm. The scalloping of the sides is an artifact of the DRIE process.

Resin-Transfer-Molding of a Tool Face

Lyndon B. Johnson Space Center, Houston, Texas

A resin-transfer-molding (RTM) process has been devised for fabricating a matrix/graphite-cloth composite panel that serves as tool face for manufacturing other composite panels. Heretofore, RTM has generally been confined to resins with viscosities low enough that they can readily flow through interstices of cloth. The present process makes it possible to use a high-temperature, more-viscous resin required for the tool face. First, a release

layer and then a graphite cloth are laid on a foam pattern that has the desired contour. A spring with an inside diameter of $3/8$ in. (≈ 9.5 mm) is placed along the long dimension of the pattern to act as a conduit for the resin. Springs with an inside diameter of $1/4$ in. (≈ 6.4 mm) are run off the larger lengthwise spring for distributing the resin over the tool face. A glass cloth is laid on top to act as breather. The whole layup is vacuum-bagged. Resin is mixed and made to flow

under vacuum assistance to infiltrate the layup through the springs. The whole process takes less than a day, and the exposure of personnel to resin vapors is minimized.

This work was done by Mike Fowler of Johnson Space Center and Edward Ehlers, David Brainard, and Charles Kellermann of ROTHE JV. For further information, contact the Johnson Commercial Technology Office at (281) 483-3809. MSC-23104

Improved Phase-Mask Fabrication of Fiber Bragg Gratings

Wavelengths and bandwidths can be tailored over wide ranges.

Marshall Space Flight Center, Alabama

An improved method of fabrication of Bragg gratings in optical fibers combines the best features of two prior methods: one that involves the use of a phase mask and one that involves interference between the two coherent laser beams. The improved method affords flexibility for tailoring Bragg wavelengths and bandwidths over wide ranges.

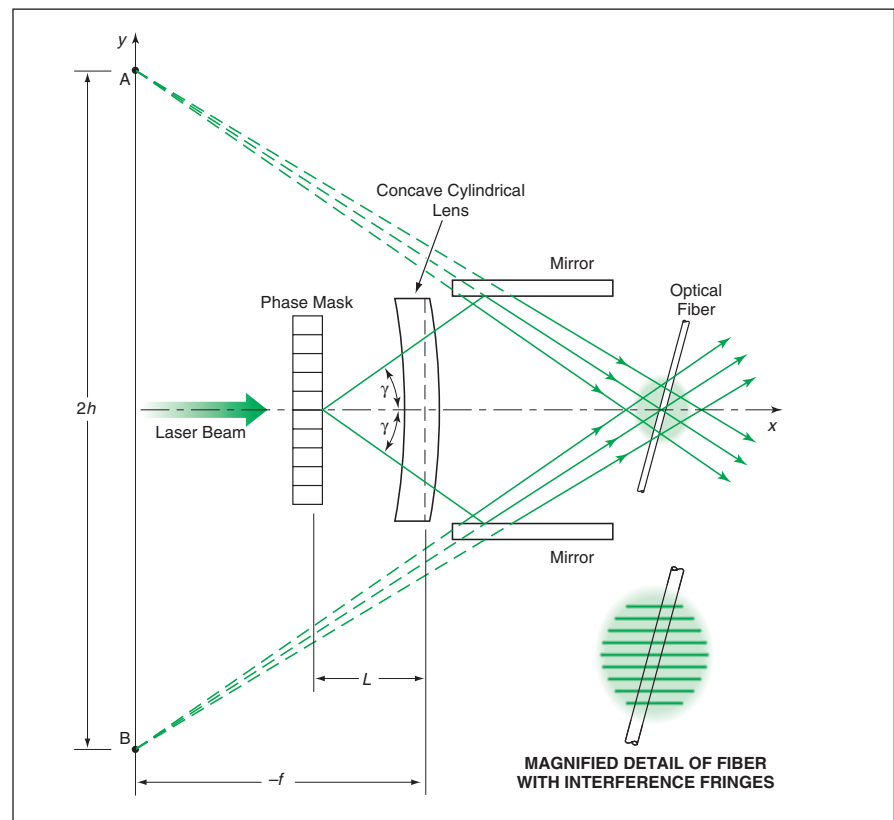
A Bragg grating in an optical fiber is a periodic longitudinal variation in the index of refraction of the fiber core. The spatial period (Bragg wavelength) is chosen to obtain enhanced reflection of light of a given wavelength that would otherwise propagate relatively unimpeded along the core. Optionally, the spatial period of the index modulation can be made to vary gradually along the grating (such a grating is said to be "chirped") in order to obtain enhanced reflection across a wavelength band, the width of which is determined by the difference between the maximum and minimum Bragg wavelengths.

In the present method as in both prior methods, a Bragg grating is formed by exposing an optical fiber to an ultraviolet-light interference field. The Bragg grating coincides with the pattern of exposure of the fiber core to ultraviolet light; in other words, the Bragg grating coincides with the interference fringes. Hence, the problem of tailoring the Bragg wavelength and bandwidth is largely one of tailoring the interference pattern and the placement

of the fiber in the interference pattern.

In the prior two-beam interferometric method, a single laser beam is split into two beams, which are subsequently recombined to produce an interference pattern at the location of an optical

fiber. In the prior phase-mask method, a phase mask is used to diffract a laser beam mainly into two first orders, the interference between which creates the pattern to which an optical fiber is exposed. The prior two-beam interfero-



An Optical Fiber Is Exposed to an interference field generated by an apparatus that affords relative insensitivity to misalignment while making it possible to select the wavelength or range of wavelengths of the Bragg grating to be formed in the fiber.

metric method offers the advantage that the period of the interference pattern can be adjusted to produce gratings over a wide range of Bragg wavelengths, but offers the disadvantage that success depends on precise alignment and high mechanical stability. The prior phase-mask method affords the advantages of compactness of equipment and relative insensitivity to both misalignment and vibration, but does not afford adjustability of the Bragg wavelength.

The present method affords both the flexibility of the prior two-beam interferometric method and the compactness and stability of the prior phase-mask method. In this method (see figure), a laser beam propagating along the x axis is normally incident on a phase mask that lies in the (y,z) plane. The phase of light propagating through the mask is modulated with a spatial periodicity, p , along the y axis chosen to diffract the laser light primarily to first order at the

angle γ . (The zero-order laser light propagating along the x axis can be used for alignment and thereafter suppressed during exposure of the fiber.) The diffracted light passes through a concave cylindrical lens, which converts the flat diffracted wave fronts to cylindrical ones, as though the light emanated from a line source. Then two parallel flat mirrors recombine the diffracted beams to form an interference field equivalent to that of two coherent line sources at positions A and B (virtual sources).

The interference pattern is a known function of the parameters of the apparatus and of position (x,y) in the interference field. Hence, the tilt, wavelength, and chirp of the Bragg grating can be chosen through suitable adjustments of the apparatus and/or of the position and orientation of the optical fiber. In particular, the Bragg wavelength can be adjusted by moving the fiber along the x axis, and the bandwidth

can be modified over a wide range by changing the fiber tilt angle or by moving the phase mask and/or the fiber.

Alignment is easy because the zero-order beam defines the x axis. The interference is relatively stable and insensitive to the mechanical vibration because of the high symmetry and compactness of the apparatus, the fixed positions of the mirrors and lens, and the consequent fixed positions of the two virtual line sources, which are independent of the translations of the phase mask and the laser relative to the lens.

This work was done by Joseph Grant of Marshall Space Flight Center and Ying Wang and Anup Sharma of Alabama Agricultural and Mechanical University.

This invention is owned by NASA, and a patent application has been filed. For further information, contact Mitch Ward, MSFC Commercialization Project Lead, at mitch.ward@nasa.gov. Refer to MFS-31596.

Tool for Insertion of a Fiber-Optic Terminus in a Connector

A grommet is protected against damage.

Lyndon B. Johnson Space Center, Houston, Texas

A tool has been developed for the special purpose of inserting the terminus of an optical fiber in a cable connector that conforms to NASA Specification SSQ-21635. What prompted the development of the tool was the observation that because of some aspects of the designs of fiber-optic termini and of springs, sealing rings, and a grommet inside the shell of such a connector, there is a tendency for the grommet to become damaged and detached from the sealing rings during installation. It is necessary to ensure the integrity of the grommet for proper seal-

ing and proper functioning of the connector. The special-purpose tool provides the needed protection for the grommet.

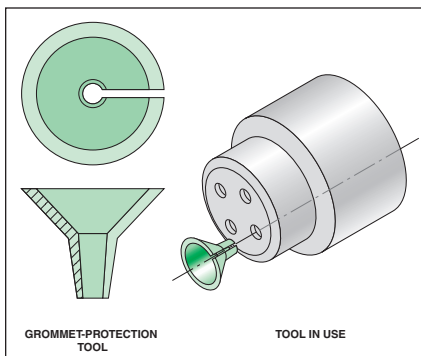
The grommet-protection tool resembles a funnel into which an axial slit has been cut (see figure). Prior to insertion, the grommet-protection tool is rolled so that one side of the slit overlaps the other side. The rolled-up grommet-protection tool is inserted in one of the connector holes that accommodate the fiber-optic termini and is pushed in until the flange (the wider of the two conical portions) of the tool becomes seated on the connector grommet. Then a special-purpose installation tool is inserted in the flange of the grommet-protection tool and pressed in until it becomes seated in the flange. This operation expands the narrower of the two conical portions of the grommet-protection tool. The installation tool is removed and the grommet-protection tool remains expanded due to the flat surfaces on the axial slit.

By use of a standard contact-insertion tool, a fiber-optic terminus is inserted, through the grommet-protection tool, into the connector cavity. By use of a pair of forceps or needle-nose pliers, the grommet-protection tool is then pulled

out of the cavity. Finally, the grommet-protection tool is removed from around the installed fiber-optic cable by pulling the cable through the axial slit.

Unlike in some prior procedures for installing the fiber-optic termini in the connector, the procedure that involves the use of the present grommet-protection tool does not include the use of lubricants that can contaminate the interior of the connector. The grommet-protection tool is made of a fluoropolymer, taking advantage of the flexibility of such polymers and further taking advantage of the inherent slipperiness of fluoropolymers. Although the tool is designed primarily for insertion of a fiber-optic terminus, it might also be useful for extracting a previously installed fiber-optic terminus.

This work was done by Wes King, Donald J. Dmonoske, John Krier, and John White of Boeing North American, Inc. for Johnson Space Center. For further information, contact Reatha H. Corbett, Patent Analyst The Boeing Company PO Box 2515 2201 Seal Beach Blvd. Seal Beach, CA 90740-1515 Phone: (562) 797-2020 E-mail: Reatha.h.corbett@boeing.com Refer to MSC-22951.



A Special-Purpose Tool Resembles a Funnel, except that it is slit along one side. It is inserted in one of the holes in the connector to protect a grommet during installation of a fiber-optic terminus in the hole.



Nanofluidic Size-Exclusion Chromatograph

This device would perform the functions of a much larger instrument.

NASA's Jet Propulsion Laboratory, Pasadena, California

Efforts are under way to develop a nanofluidic size-exclusion chromatograph (SEC), which would be a compact, robust, lightweight instrument for separating molecules of interest according to their sizes and measuring their relative abundances in small samples. About as large as a deck of playing cards, the nanofluidic SEC would serve, in effect, as a "laboratory on a chip" that would perform the functions of a much larger, conventional, bench-top SEC and ancillary equipment, while consuming much less power and much smaller quantities of reagent and sample materials. Its compactness and low power demand would render it attractive for field applications in which, typically, it would be used to identify and quantitate a broad range of polar and nonpolar organic compounds in soil, ice, and water samples.

Size-exclusion chromatography is a special case of high-performance liquid chromatography. In a conventional SEC, a sample plug is driven by pressure along a column packed with silica or polymer beads that contain uniform nanopores. The interstices between, and the pores in, the beads collectively constitute a size-exclusion network. Molecules follow different paths through the size-exclusion network, such that characteristic elution

times can be related to sizes of molecules: basically, smaller molecules reach the downstream end of the column after the larger ones do because the smaller ones enter minor pores and stay there for a while, whereas the larger ones do not enter the pores. The volume accessible to molecules gradually diminishes as their size increases. All molecules bigger than a pore size elute together. For most substances, the elution times and sizes of molecules can be correlated directly with molecular weights. Hence, by measuring the flux of molecules arriving at the downstream end as a function of time, one can obtain a liquid mass spectrum for the molecules present in a sample over a broad range of molecular weights.

The developmental nanofluidic SEC is based on the same size-separation principle as that of a conventional SEC. However, instead of a packed macroscopic column containing porous beads, the nanofluidic SEC would contain a size-exclusion network in a miniature column in the form of a microscopic channel containing nanometer-scale features (see figure). More specifically, the nanometer-scale features in the channel would be sized, shaped, and positioned to define a matrix of micron-width subchannels topped with a gap of varying thick-

ness of the order of tens of nanometers. The miniature column would be fabricated by established techniques now used to produce integrated circuits (ICs) and microelectromechanical systems (MEMS). One or more device(s) to detect molecules could be integrated onto the column chip at the downstream end. These devices could be based, for example, on electrochemical (in particular, amperometric) and laser-induced-fluorescence detection techniques.

This work was done by Sabrina Feldman, Danielle Svehla, Frank Grunthaner, Jason Feldman, and P. Shakkottai of Caltech for NASA's Jet Propulsion Laboratory. Further information is contained in a TSP (see page 1).

In accordance with Public Law 96-517, the contractor has elected to retain title to this invention. Inquiries concerning rights for its commercial use should be addressed to:

Intellectual Assets Office

JPL

Mail Stop 202-233

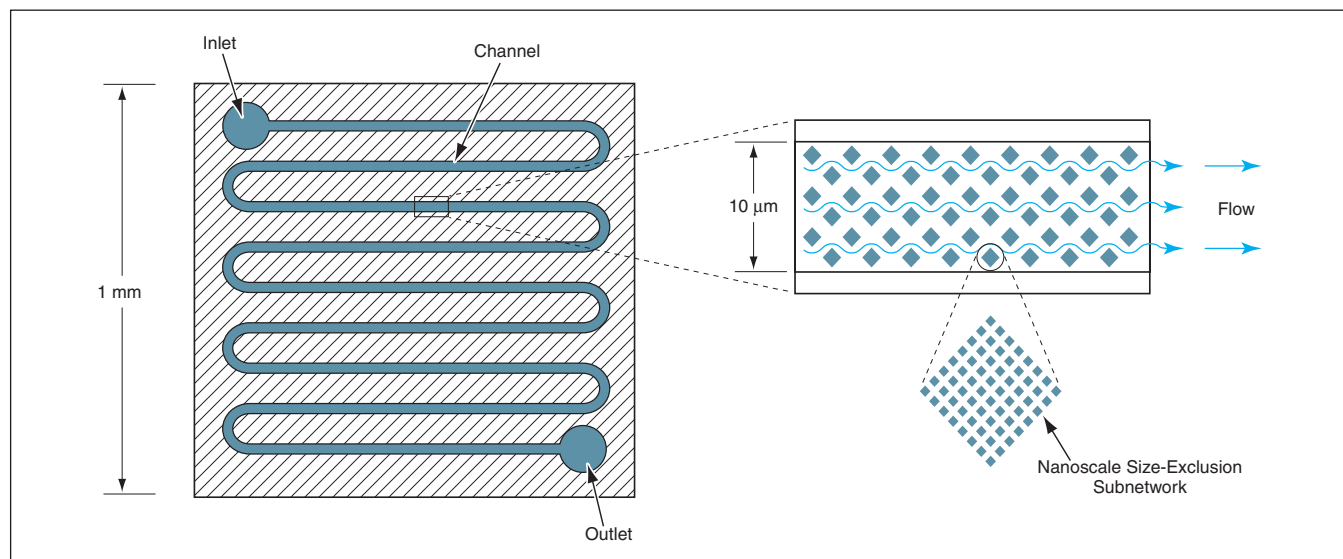
4800 Oak Grove Drive

Pasadena, CA 91109-8099

(818) 354-2240

E-mail: ipgroup@jpl.nasa.gov

Refer to NPO-30499, volume and number of this NASA Tech Briefs issue, and the page number.



A Size-Separation Network in a Miniature Channel on a chip would contain nanoscale features. The channel and features would be formed as one piece in a chip by use of IC and MEMS fabrication techniques.

Lightweight, Low-CTE Tubes Made From Biaxially Oriented LCPs

CTEs can be tailored by tailoring biaxial orientations.

John H. Glenn Research Center, Cleveland, Ohio

Tubes made from biaxially oriented liquid-crystal polymers (LCPs) have been developed for use as penetrations on cryogenic tanks. ("Penetrations" in this context denotes feed lines, vent lines, and sensor tubes, all of which contribute to the undesired conduction of heat into the tanks.) In comparison with corresponding prior cryogenic-tank penetrations made from stainless steels and nickel alloys, the LCP penetrations offer advantages of less weight and less thermal conduction. An additional major advantage of LCP components is that one can tailor their coefficients of thermal expansion (CTEs). The estimated cost of continuous production of LCP tubes of typical sizes is about \$1.27/ft (\$4.17/m) [based on 1998 prices].

LCP tubes that are compatible with liquid oxygen and that feature tailored biaxial molecular orientation and quasi-isotropic properties (including quasi-isotropic CTE) have been fabricated by a combination of proprietary and patented techniques that involve the use of counterrotating dies (CRDs). Tailoring of the angle of molecular orientation is what makes it possible to tailor the CTE

over a wide range to match the CTEs of adjacent penetrations of other tank components; this, in turn, makes it possible to minimize differential-thermal expansion stresses that arise during thermal cycling.

The fabrication of biaxially oriented LCP tubes by use of CRDs is not new in itself. The novelty of the present development lies in tailoring the orientations and thus the CTEs and other mechanical properties of the LCPs for the intended cryogenic applications and in modifications of the CRDs for this purpose.

The LCP tubes and the 304-stainless-steel tubes that the LCP tubes were intended to supplant were tested with respect to burst strength, permeability, thermal conductivity, and CTE. The following conclusions were drawn from the tests:

- The thermal conductivities of the LCP tubes ranged from 0.21 to 0.40 W/(m·K) — 98 percent smaller than those of the corresponding 304-stainless-steel tubes.
- The CTEs of the LCPs were fully tailorable down to an exceptionally low value of $5.8 \times 10^{-6} (\text{°C})^{-1}$.
- It was necessary to fabricate an LCP tube with a wall thickness of 0.080 in.

(≈ 2.0 mm) to obtain a flexural strength equal to that of a 304-stainless-steel tube with a wall thickness of 0.028 in. (≈ 0.7 mm). Even with its greater thickness, the LCP tube weighed 53 percent less than did the stainless-steel tube.

- The LCP tubes exhibited exceptionally low permeability: The average rate of transport of oxygen through an LCP tube having dimensions typical of those of a cryogenic tank at a temperature of -183 °C was found to be of the order of $4 \times 10^{-21} \text{ cm}^3$ (standard temperature and pressure) per day.
- All of the LCP tubes exceeded the hydrostatic-burst-strength requirement by at least 400 percent.

This work was done by Leslie Rubin, Frank Federico, Richard Formato, John Larouco, and William Slager of Foster-Miller, Inc., for Glenn Research Center.

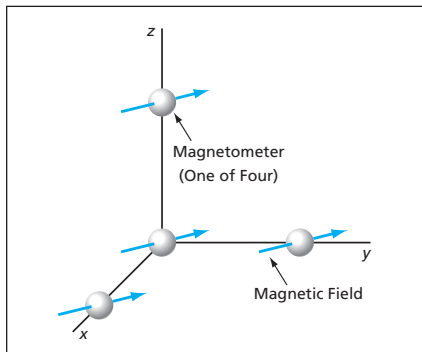
Inquiries concerning rights for the commercial use of this invention should be addressed to NASA Glenn Research Center, Commercial Technology Office, Attn: Steve Fedor, Mail Stop 4-8, 21000 Brookpark Road, Cleveland Ohio 44135. Refer to LEW-16780.

Using Redundancy To Reduce Errors in Magnetometer Readings

Fundamental laws of electromagnetism impose constraints that can be exploited.

NASA's Jet Propulsion Laboratory, Pasadena, California

A method of reducing errors in noisy magnetic-field measurements involves exploitation of redundancy in the readings of multiple magnetometers in a cluster.



Four Magnetometers at corners of a cube provide noisy, redundant measurements of a magnetic field. The redundancy can be used to partly correct for the noise contributions.

By "redundancy" is meant that the readings are not entirely independent of each other because the relationships among the magnetic-field components that one seeks to measure are governed by the fundamental laws of electromagnetism as expressed by Maxwell's equations.

Assuming that the magnetometers are located outside a magnetic material, that the magnetic field is steady or quasi-steady, and that there are no electric currents flowing in or near the magnetometers, the applicable Maxwell's equations are

$$\nabla \times \mathbf{B} = 0 \text{ and } \nabla \cdot \mathbf{B} = 0,$$

where \mathbf{B} is the magnetic-flux-density vector. By suitable algebraic manipulation, these equations can be shown to impose three independent constraints on the values of the components of \mathbf{B} at the various magnetometer positions.

In general, the problem of reducing the errors in noisy measurements is one of finding a set of corrected values that minimize an error function. In the present method, the error function is formulated as (1) the sum of squares of the differences between the corrected and noisy measurement values plus (2) a sum of three terms, each comprising the product of a Lagrange multiplier and one of the three constraints. The partial derivatives of the error function with respect to the corrected magnetic-field component values and the Lagrange multipliers are set equal to zero, leading to a set of equations that can be put into matrix-vector form. The matrix can be inverted to solve for a vector that comprises the corrected magnetic-field component values and the Lagrange multipliers.

The method was tested in computational simulations of random noise superimposed on readings of a dipole magnetic field by four magnetometers in a cluster like the one shown in the figure.

The numerical results of the simulations showed that errors in the magnetometer readings were reduced by values ranging from about 20 to about 40 percent.

This work was done by Igor Kulikov and Michail Zak of Caltech for NASA's Jet Propulsion Laboratory. Further information is contained in a TSP (see page 1).NPO-40695

Compact Instrument for Measuring Profile of a Light Beam

A simple optical assembly is combined with a conventional CCD beam profiler.

Lyndon B. Johnson Space Center, Houston, Texas

The beamviewer is an optical device designed to be attached to a charge-coupled-device (CCD) image detector for measuring the spatial distribution of intensity of a beam of light (the "beam profile") at a designated plane intersecting the beam. The beamviewer-and-CCD combination is particularly well suited for measuring the radiant-power profile (for a steady beam) or the radiant-energy profile (for a pulsed beam) impinging on the input face or emerging from the output face of a bundle of optical fibers. The beamviewer-and-CCD combination could also be used as a general laboratory instrument for profiling light beams, including beams emerging through small holes and laser beams in free space.

There are numerous commercial beam-profiling instruments, but each is deficient in one or more respects that include, variously, low dynamic range, optomechanical complexity, large size, difficulty of alignment, and/or high cost. In contrast, the beamviewer is compact, easy to align, capable of operation over a wide dynamic range, and relatively inexpensive.

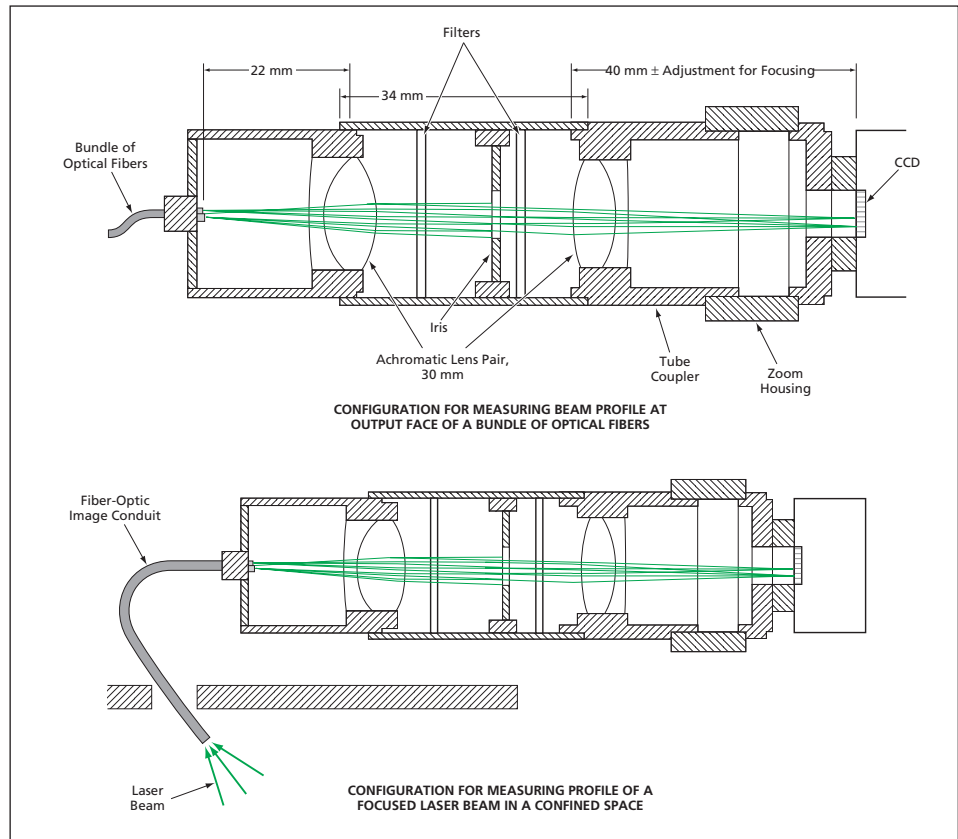
The beamviewer is designed to be attached to the optical mount on the CCD portion of any off-the-shelf CCD beam profiler. The figure depicts the beamviewer-and-CCD combination as configured for measuring the beam profile at the output face of a bundle of optical fibers. The beamviewer includes an achromatic lens pair arranged in a telecentric system, such that an image of the output face of the fiber-optic bundle is projected onto the CCD with a desired amount of magnification. An iris between the lenses can be used to control the light flux and the depth of focus. There are also spaces between the lenses for inserting

neutral-density filters to attenuate powerful light beams to protect the CCD against damage and prevent saturation of its output. By using or refraining from using the iris, the neutral-density filters, and the electronic control of the CCD gain and shutter speed of the off-the-shelf beam profiler, it is possible to attain a dynamic range of 10^{10} .

The beamviewer configuration for measuring the profile of a beam at a plane other than the output face of a fiber-optic bundle is the same as that described above, except for the input coupling. In this case, the output face of a fiber-optic image conduit (a fused fiber-optic bundle with polished end faces

that consists of 3- μm fibers, each fiber acts like a pixel) is placed at the input focal plane of the telecentric lens system, and the input plane of the fiber-optic image conduit is placed in the plane where the beam profile is to be measured. The light-intensity distribution at the input face of the conduit is reproduced (with some attenuation) at the output face, then imaged on the CCD as described above.

This work was done by Valeri Papanyan of Lockheed Martin Corp. for Johnson Space Center. For further information, contact the Johnson Commercial Technology Office at (281) 483-3809. MSC-23553



The **Achromatic Lens Pair** projects a magnified image of the cross section of a light beam onto a CCD for measurement of the spatial distribution of light in the cross section.

Multilayer Dielectric Transmissive Optical Phase Modulator

Full-cycle phase change with low distortion would be produced over a terahertz optical bandwidth.

Marshall Space Flight Center, Alabama

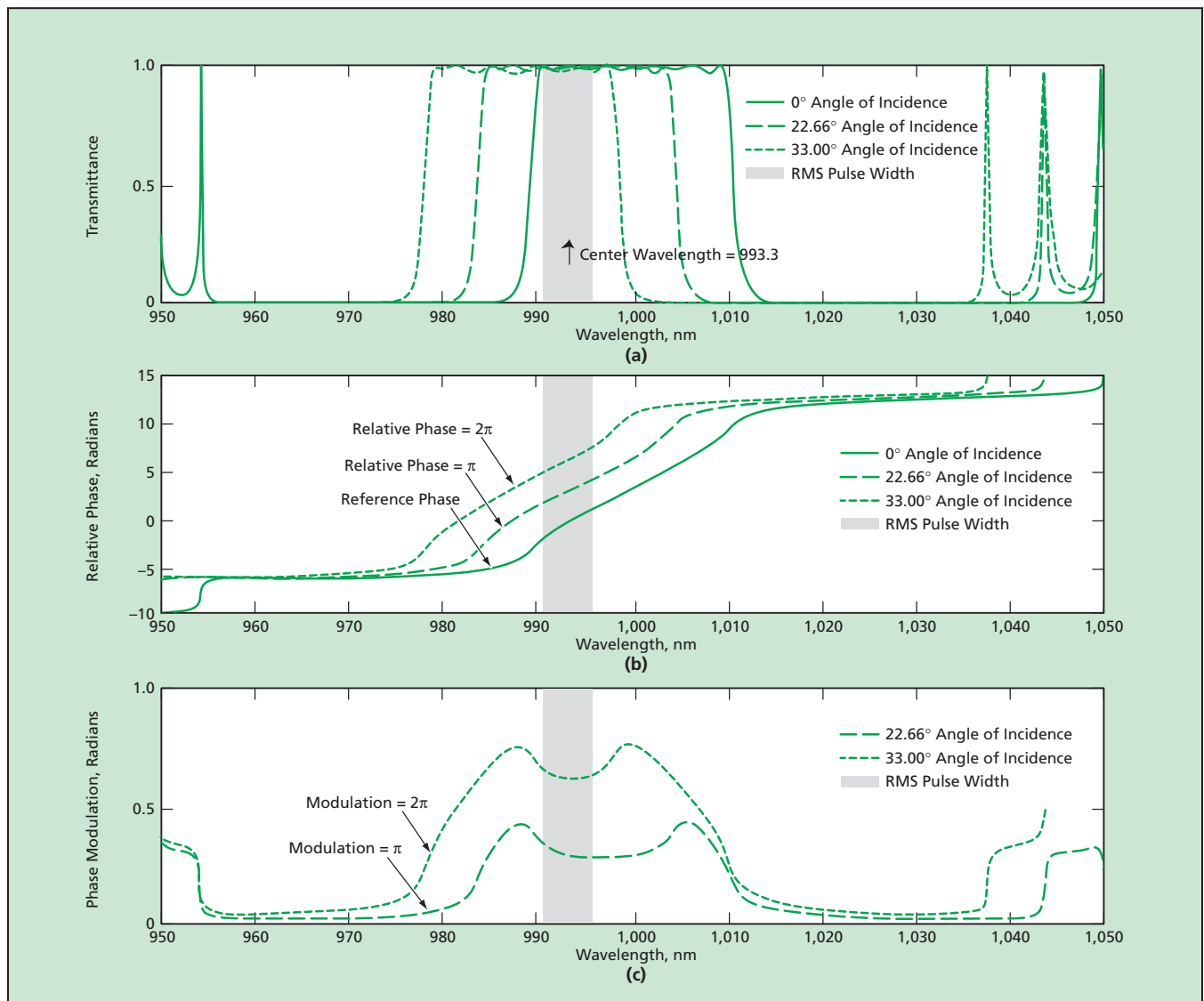
A multilayer dielectric device has been fabricated as a prototype of a low-loss, low-distortion, transmissive optical phase modulator that would provide as much as a full cycle of phase change for all frequency components of a transmitted optical pulse over a frequency band as wide as 6.3 THz. Arrays of devices like this one could be an alternative to the arrays of mechanically actuated phase-control optics (adaptive optics) that have heretofore been used to correct for wave-front distortions in highly precise optical systems. Potential applications for these high-speed wave-front-control arrays of devices include agile beam steering, optical com-

munications, optical metrology, optical tracking and targeting, directional optical ranging, and interferometric astronomy.

The device concept is based on the same principle as that of band-pass interference filters made of multiple dielectric layers with fractional-wavelength thicknesses, except that here there is an additional focus on obtaining the desired spectral phase profile in addition to the device's spectral transmission profile. The device includes a GaAs substrate, on which there is deposited a stack of GaAs layers alternating with AlAs layers, amounting to a total of 91 layers. The design thicknesses of the layers range from

10 nm to $>1 \mu\text{m}$. The number of layers and the thickness of each layer were chosen in a computational optimization process in which the wavelength dependences of the indices of refraction of GaAs and AlAs were taken into account as the design was iterated to maximize the transmission and minimize the group-velocity dispersion for a wavelength band wide enough to include all significant spectral components of the pulsed optical signal to be phase modulated.

The figure depicts the normal-incidence power transmission and relative transmitted phase spectrum computed for the optimized design. The band-pass re-



The Computed Transmittance Spectrum (a) and Relative Phase Spectrum (b) of the proposed device indicate the ability to phase-modulate an optical signal without changing transmission levels. The Phase Modulation Spectrum (c) shows full cycle phase modulation levels across the full spectral pulse width.

gion — about 21 nm wide in wavelength and 6.3 THz wide in frequency — would feature an edge-to-edge phase change of 2.08 full cycles — slightly greater than 4 radians. The large edge-to-edge phase change would create the potential for any level of phase modulation, provided that one could select a modulation technique that would shift the transmission function far enough in the appropriate direction.

Computational tests were performed for an input optical signal with a Gaussian amplitude envelope, a center wavelength of 993.3 nm, and a root-mean-square (rms) wavelength width of 5 nm, corresponding to pulse duration of 52 fs. One reason for this choice of parameters is that it positions the rms bandwidth of the signal within the shorter-wavelength half of the transmission pass band of the device with the center wavelength at the peak of the second transmission resonance ripple. Another reason for this choice of parameters is that it provides for all significant frequency components

of the signal to have access to a full cycle of phase modulation without adversely affecting transmission levels.

An appropriate modulation technique would enable the wavelength shift of the transmission function such that the signal would be shifted from lower half of the pass band to the upper half of the pass band; this amount of shift would bring all significant frequency components of the signal through a complete cycle of phase modulation. In order for this modulation scheme to be successful, the wavelength shift of the transmission must not change the shape of this function in the pass band. The fabricated prototype device has been characterized in its ability to affect transmission phase through a mechanical change in the signal's angle of incidence.

Nonmechanical modulation would likely be effected by an electrorefractive or nonlinear optical technique that would vary the indices of refraction of the GaAs and AlAs layers. The technique has not yet been selected. A computational simula-

tion has shown that a decrease of 1.3 percent in the indices of refraction of the GaAs and AlAs layers would shift the transmission function to shorter wavelengths by an amount sufficient to provide a full cycle of phase modulation for the 993.3-nm test signal. The simulation also showed that a similarly sized increase in the indices of refraction would shift the transmission function to longer wavelengths by an amount sufficient to put the test signal in a wavelength region of high reflectivity; taking advantage of this behavior, one could use the device as an optical switch.

This work was done by Andrew Scott Keys of Marshall Space Flight Center and Richard Lynn Fork of the University of Alabama in Huntsville. Further information is contained in a TSP (see page 1).

This invention is owned by NASA, and a patent application has been filed. For further information, contact Jim Dowdy, MSFC Commercialization Assistance Lead, at jim.dowdy@nasa.gov. Refer to MFS-31565.

Second-Generation Multi-Angle Imaging Spectroradiometer

NASA's Jet Propulsion Laboratory, Pasadena, California

A report discusses an early phase in the development of the MISR-2 C, a second, improved version of the Multi-angle Imaging SpectroRadiometer (MISR), which has been in orbit around the Earth aboard NASA's Terra spacecraft since 1999. Like the MISR, the MISR-2 would contain a "pushbroom" array of nine charge-coupled-device (CCD) cameras — one aimed at the nadir and the others aimed at different angles sideways from the nadir. The major improvements embodied in the MISR-2 would be the following:

- A new folded-reflective-optics design would render the MISR-2 only a third as massive as the MISR.
- Smaller filters and electronic circuits would enable a reduction in volume to a sixth of that of the MISR.
- The MISR-2 would generate images in two infrared spectral bands in addition to the blue, green, red, and near-infrared spectral bands of the MISR.
- Miniature polarization filters would be incorporated to add a polarization-sensing capability.

- Calibration would be performed non-intrusively by use of a gimbaled tenth camera.

The main accomplishment thus far has been the construction of an extremely compact all-reflective-optics CCD camera to demonstrate feasibility.

This work was done by Steven Macenka, Larry Hovland, Daniel Preston, Brian Zellers, and Kevin Downing of Caltech for NASA's Jet Propulsion Laboratory. Further information is contained in a TSP (see page 1). NPO-35097

Real-Time Adaptive Color Segmentation by Neural Networks

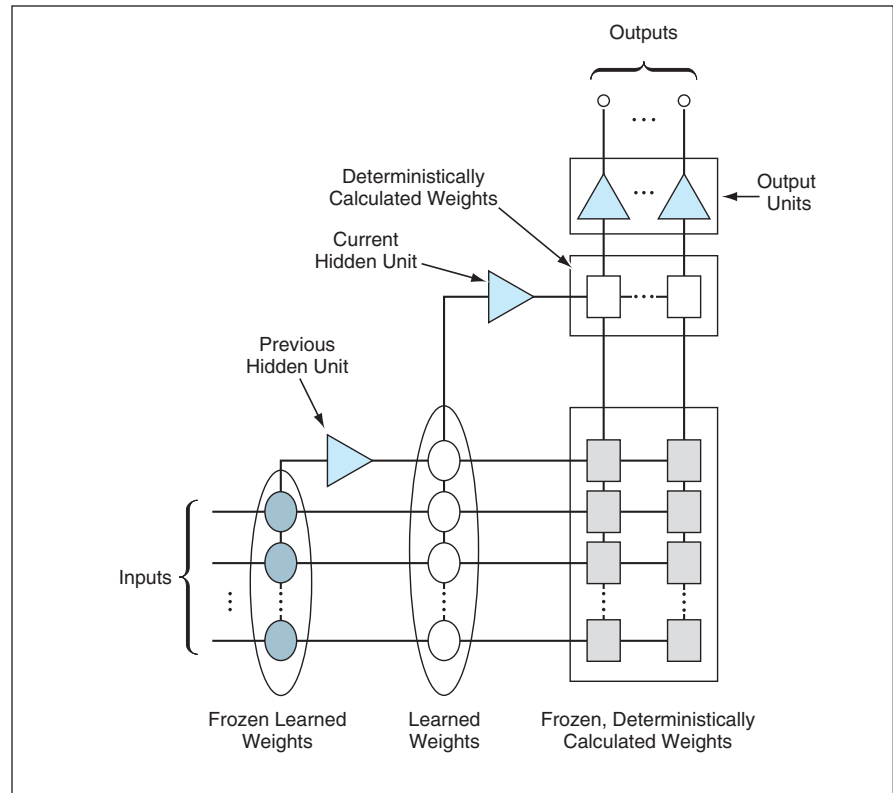
Changing images would be analyzed to detect features of interest.

NASA's Jet Propulsion Laboratory, Pasadena, California

Artificial neural networks that would utilize the cascade error projection (CEP) algorithm have been proposed as means of autonomous, real-time, adaptive color segmentation of images that change with time. In the original intended application, such a neural network would be used to analyze digitized color video images of terrain on a remote planet as viewed from an uninhabited spacecraft approaching the planet. During descent toward the surface of the planet, information on the segmentation of the images into differently colored areas would be updated adaptively in real time to capture changes in contrast, brightness, and resolution, all in an effort to identify a safe and scientifically productive landing site and provide control feedback to steer the spacecraft toward that site. Potential terrestrial applications include monitoring images of crops to detect insect invasions and monitoring of buildings and other facilities to detect intruders.

The CEP algorithm is reliable and is well suited to implementation in very-large-scale integrated (VLSI) circuitry. It was chosen over other neural-network learning algorithms because it is better suited to real-time learning: It provides a self-evolving neural-network structure, requires fewer iterations to converge and is more tolerant to low resolution (that is, fewer bits) in the quantization of neural-network synaptic weights. Consequently, a CEP neural network learns relatively quickly, and the circuitry needed to implement it is relatively simple.

Like other neural networks, a CEP neural network includes an input layer, hidden units, and output units (see figure). As in other neural networks, a CEP network is presented with a succession of input training patterns, giving rise to a set of outputs that are compared with the desired outputs. Also as in other neural networks, the synaptic weights are updated iteratively in an effort to bring the outputs closer to target values. A distinctive feature of the CEP neural network and algorithm is that each update of synaptic weights takes place in conjunction with the addition of another hidden unit, which then re-



A CEP Neural Network, depicted here in simplified form, is well suited to real-time learning and to implementation in VLSI circuitry.

mains in place as still other hidden units are added on subsequent iterations. For a given training pattern, the synaptic weight between (1) the inputs and the previously added hidden units and (2) the newly added hidden unit is updated by an amount proportional to the partial derivative of a quadratic error function with respect to the synaptic weight. The synaptic weight between the newly added hidden unit and each output unit is given by a more complex function that involves the errors between the outputs and their target values, the transfer functions (hyperbolic tangents) of the neural units, and the derivatives of the transfer functions.

The adaptive color-segmentation process of a proposed CEP can be summarized as follows: The knowledge acquired by the network up to a given time, t_0 , would be used in segmenting the image at the next increment of time,

$t_0 + \Delta t$. The results of the segmentation at $t_0 + \Delta t$ would then be used to update the knowledge pertaining to time t_0 . This segmentation and updating would be performed repeatedly as new imagery was acquired.

On the basis of (1) computational simulations using representative terrain images and (2) the performances of prior CEP integrated circuits, it has been estimated that adaptive learning can be achieved in times of the order of milliseconds. An important issue that must be addressed in practical development is how often updates must be performed: The frequency of updates would directly affect the power demand of the proposed CEP circuitry.

This work was done by Tuan A. Duong of Caltech for NASA's Jet Propulsion Laboratory. Further information is contained in a TSP (see page 1). NPO-30692



Research and Development in Optical Communications

A report in the form of lecture slides summarizes the optical-communications program of NASA's Jet Propulsion Laboratory (JPL) and describes the JPL Optical Communications Telescope Laboratory (OCTL) and its role in the program. The purpose of the program is to develop equipment and techniques for laser communication between (1) ground stations and (2) spacecraft (both near Earth and in deep space) and aircraft. The OCTL is an astronomical-style telescope facility that includes a 1-m-diameter, 75.8-m-focal length telescope in an elevation/azimuth mount, plus optical and electronic subsystems for tracking spacecraft and aircraft, receiving laser signals from such moving targets, and transmitting high-power laser signals to such targets. Near-term research at the OCTL is expected to focus on mitigating the effects of atmospheric scintillation on uplinks and on beacon-assisted tracking of ground stations by stations in deep space. Near-term experiments are expected to be performed with retroreflector-equipped aircraft and Earth-orbiting spacecraft techniques to test mathematical models of propagation of laser beams, multiple-beam strategies to mitigate uplink scintillation, and pointing and tracking accuracy of the telescope.

*This work was done by Keith Wilson of Caltech for NASA's Jet Propulsion Laboratory. Further information is contained in a TSP (see page 1).
NPO-30575*

Tests of Multibeam Scintillation Mitigation on Laser Uplinks

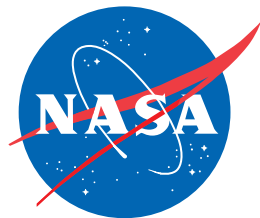
A report presents additional details about parts of the program of research and development that is the topic of the immediately preceding article. The report emphasizes those aspects of the program that pertain to the use of multiple uplink laser beams in a ground-to-spacecraft optical communication system to reduce (relative to the case of a single uplink laser beam) the depth and frequency of occurrence of fades in the uplink signal received at the spacecraft. The underlying multibeam scintillation-mitigation concept was described in "Multiple-Beam Transmission for Optical Communication" (NPO-20384), *NASA Tech Briefs*, Vol. 22, No. 11 (November 1998), page 56. The report discusses the need for mitigating uplink scintillation; briefly describes the Optical Communications Telescope Laboratory and its role as the ground station in the research; summarizes prior experiments in uplink scintillation and multibeam mitigation of scintillation in ground-to-spacecraft laser communications; and describes key experiments planned to be performed in the next five years. The report then elaborates somewhat on the initial experiments, which are to be dedicated to understanding and perfecting the multibeam scintillation-mitigation strategy.

*This work was done by Keith Wilson of Caltech for NASA's Jet Propulsion Laboratory. Further information is contained in a TSP (see page 1).
NPO-30548*

Spaceborne Infrared Atmospheric Sounder

A report describes the development of the spaceborne infrared atmospheric sounder (SIRAS) — a spectral imaging instrument, suitable for observing the atmosphere of the Earth from a spacecraft, that utilizes four spectrometers to cover the wavelength range of 12 to 15.4 μm with a spectral resolution that ranges between 1 part per 900 and 1 part per 1,200 in wavelength. The spectrometers are operated in low orders to minimize filtering requirements. Focal planes receive the dispersed energy and provide a spectrum of the scene. The design of the SIRAS combines advanced, wide-field refractive optics with high-dispersion gratings in a solid-state (no moving parts), diffraction-limited optical system that is the smallest such system that can be constructed for the specified wavelength range and resolution. The primary structure of the SIRAS has dimensions of 10 by 10 by 14 cm and has a mass of only 2.03 kg.

*This work was done by Thomas Pagano, Steven Macenka, and Thomas Kampe of Caltech for NASA's Jet Propulsion Laboratory. Further information is contained in a TSP (see page 1).
NPO-30202*



National Aeronautics and
Space Administration